Highly Efficient Magnetic Phosphoric Acid Modified Defatted Chlorella Vulgaris Algae (MDCV/Fe3O4) as a Novel Biosorbent for Methylene Blue Removal

Zeinab Salehi (zsalehy@ut.ac.ir)
University of Tehran
Sahar Naziri
University of Tehran

Research

Keywords: Chlorella vulgaris, Lipid extraction, Phosphoric acid modification, magnetic composite, Methylene blue biosorption

Posted Date: January 4th, 2021

DOI: https://doi.org/10.21203/rs.3.rs-136792/v1

Highly efficient magnetic phosphoric acid modified defatted *Chlorella vulgaris* algae (MDCV/Fe_3O_4) as a novel biosorbent for methylene blue removal

Sahar Naziri[1], Zeinab Salehi*[2]

[1] Department of Chemical Engineering, School of Chemical Engineering, College of Engineering, University of Tehran, Tehran, Iran

Corresponding author's email: zsalehy@ut.ac.ir

Abstract

Background:

A novel biosorbent based on defatted *Chlorella vulgaris* (DCV) as a by-product of the biofuel industry was considered as an economical and inexpensive biosorbent in the form of magnetic modified defatted *Chlorella vulgaris* (MDCV/Fe3O4) for methylene blue (MB) removal. The lipid extraction was performed on raw *Chlorella vulgaris* (RCV). Phosphoric acid was selected as a DCV modifier. During acid modification, the variables affecting the biosorption capacity and the residual algae such as temperature (30-70 ℃), the contact time of DCV with acid (3-9 hr), the concentration of acid (2-6 mol/L), and the ratio of acid volume to DCV (30-70 mL/g) were investigated and optimized using Minitab-18 software. The modified defatted *Chlorella vulgaris* (MDCV) was prepared by acidification of DCV under optimal conditions. MDCV/Fe_3O_4 was prepared using the co-precipitation method for easy and low-cost separation of biosorbent. The XRD, FTIR, SEM, EDS, BET, and VSM analyses were performed to identify the structures and characteristics of RCV, DCV, MDCV, and MDCV/Fe_3O_4. Some experiments were designed using Minitab-18 software to investigate the effects of temperature (5-45 ℃), contact time (30-90 min), biosorbent dosage (15-45 mg), initial concentration of MB (20-100 mg/L), and pH (5-9) on the biosorption capacity of MDCV/Fe_3O_4. The kinetic, isothermal and thermodynamic parameters were investigated on MDCV/Fe_3O_4.

Results:

The specific surface area of MDCV/Fe_3O_4 was 25.20 m^2/g. RCV, DCV, and MDCV/Fe_3O_4 had a crystalline structure and MDCV had an amorphous structure. The data were most consistent with Pseudo-second-order and Freundlich models. The maximum biosorption capacity of MDCV/Fe_3O_4 was calculated in the amount of 32.44 mg/g. According to the positive values of ΔG and negative values of ΔH (-46.56 kJ/mol) and ΔS (-0.17 kJ/mol.K), the biosorption of MB on MDCV/Fe_3O_4 was non-spontaneous, exothermic with a decrease in irregularity.

Conclusions:

In this study, MDCV/Fe_3O_4 was applied as the MB biosorbent. Modifications such as lipid extraction, phosphoric acid modification and magnetization improved this biosorbent in its biosorption capacity and separation. Data were optimized in the acid modification and MB biosorption steps. Comparison of the characteristics of MDCV/Fe_3O_4 with unmodified species confirmed its high efficiency. Kinetic, isothermal and thermodynamic studies were also performed.

Keywords:

Chlorella vulgaris, Lipid extraction, Phosphoric acid modification, magnetic composite, Methylene blue biosorption

Background

Water is one of the main human needs that the development of urbanization and industry has polluted. Among organic pollutants, dyes are one of the important toxic with destructive effects, causing global attentions [1]. They have negative influences on the health of aquatic organisms and the passage of light into the water for plants' photosynthesis. In addition, they are very carcinogenic due to their aromatic structure, which poses a serious threat to human and animal health [2]. Artificial dyes are used in various industries such as textiles, plastics, foods, medicines, etc. [3]. Methylene blue (MB) is a cationic dye with detrimental effects on organisms over a short time [4]. It has morbidities such as eye irritation, headache, nausea, dizziness, and excessive sweating [5]. Therefore, the treatment of wastewater containing this dye is very significant due to its harmful effects.

Hitherto, various physical and chemical methods such as filtration, coagulation, flocculation, irradiation, oxidation, catalytic ozonation, etc, have been used to separate organic pollutants from effluents [6-11]. Environmental hazards, high operating costs, more time consuming, and requiring special expensive equipment are some of the disadvantages of these methods [12]. So, it is important to develop efficient, inexpensive, environmentally friendly, and high-efficiency methods.

The biosorption methods using biochars due to environmental compatibility, non-toxicity, low price, availability, and abundance are suitable for removing organic pollutants [13]. Some studies have suggested the use of biosorbents such as banana, cucumber, and potato peel [14], sago [15], leaves [16], rice husk [17], egg shell [18], and diverse algae such as *Sargassum dentifolium*, *Ulva fasciata* [19], *Chlorella pyrenoidosa* [20], *Scenedesmus* [21], and *Spirulina* [22]. These biosorbents are very efficient and inexpensive for the removal of organic pollutants from industrial effluents. However, the separation of these biosorbents is difficult and costly. Therefore, research was done on magnetizing the adsorbents as a cheap, effective, and easy separable material [23].

Chlorella vulgaris is biomass with high potential in biofuel production and as a by-product in the biofuel industry can be used for adsorbing many urban, industrial, and agricultural pollutants such as heavy metals, dyes, and pharmaceutical pollutants. This algae grows rapidly and its

structure is resistant to adverse conditions. They are also a source of substances such as lipids, carbohydrates, proteins, vitamins, pigments, and minerals. Growth conditions such as limited nitrogen and phosphorus sources, high levels of carbon dioxide, light intensity and temperature increase the level of lipids and starches [24]. The fatty acids in polar lipid cell membranes and non-polar lipids, as energy sources, are used in the biodiesel production process and directly affect its quality [25].

Some researchers have shown that the extraction of lipids from algae increases the specific surface area and its biosorption capacity [26, 27]. On the other hand, there are studies on the use of sulfuric acid, hydrochloric acid, phosphoric acid, boric acid, etc, as a pretreatment of algae to increase biosorption capacity [28, 29].

One of the important issues is the efficient and low-cost separation of the biosorbents after the biosorption process. For this purpose, there are some studies on magnetic biological materials from different sources such as magnetic *Sargassum horneri* [30], magnetic *Cymopolia barbata* [31], and magnetic activated carbon [32].

In this study extraction of the lipid from raw *Chlorella vulgaris* (RCV) and modification of defatted *Chlorella vulgaris* (DCV) was carried out to gain further MB biosorption. Then it was subjected to an acid modification to increase the specific surface area of DCV. Another goal is magnetizing the modified defatted *Chlorella vulgaris* (MDCV) for easy and low-cost separation. In the acid treatment step, the variables affecting the MDCV biosorption capacity and residual MDCV were modeled by Minitab-18 software, using the response surface methodology (RSM). The magnetic modified defatted *Chlorella vulgaris* (MDCV/Fe_3O_4) was prepared as the final biosorbent. In the end, the effect of variables on the biosorption capacity of MDCV/Fe_3O_4, was considered and modeled by Minitab-18 software. Finally, kinetic, isotherm, and thermodynamic parameters were studied.

Results and discussion

Phosphoric acid treatment and optimization of parameters

In order to optimize variables of acid treatment, the experimental results of the proposed levels are reported in Table 1. Also, multiple regression analysis of experimental data with 95% probability

has been reported in Equations 1-2. Ineffective variables were removed to increase the suitability of the models with experimental data [33].

Table (1) - Experimental results from CCD proposed levels

Run no.	X_1, T	X_2, t	X_3, C_A	X_4, V/W	Y_1, q_{MDCV}	Y_2, RP_{MDCV}
1	-1	-1	-1	-1	8.2250	56.5
2	1	-1	-1	-1	9.1465	45.5
3	-1	1	-1	-1	9.8998	52.5
4	1	1	-1	-1	10.6434	31.0
5	-1	-1	1	-1	10.4720	52.5
6	1	-1	1	-1	8.8975	22.5
7	-1	1	1	-1	9.3889	46.5
8	1	1	1	-1	7.8629	10.0
9	-1	-1	-1	1	6.8480	53.5
10	1	-1	-1	1	8.2671	49.5
11	-1	1	-1	1	7.7110	57.5
12	1	1	-1	1	9.7640	30.0
13	-1	-1	1	1	10.4203	45.5
14	1	-1	1	1	10.5270	20.5
15	-1	1	1	1	9.9386	51.5
16	1	1	1	1	10.6725	9.5
17	-1	0	0	0	9.5086	50.5
18	1	0	0	0	11.6263	23.0
19	0	-1	0	0	11.3029	52.0
20	0	1	0	0	11.1090	46.0

21	0	0	-1	0	11.4420	51.0
22	0	0	1	0	11.9916	46.5
23	0	0	0	-1	12.8031	49.5
24	0	0	0	1	12.4863	47.0
25	0	0	0	0	12.7223	48.0
26	0	0	0	0	12.6818	48.0
27	0	0	0	0	12.8035	47.5

$$Y_1 = -5.02 + 0.4863X_1 + 2.047X_2 + 0.504X_3 - 0.1110X_4 - 0.004711X_1^2 - 0.1384X_2^2 - 0.01156X_1X_3 + 0.000898X_1X_4 - 0.0832X_2X_3 + 0.01603X_3X_4 \quad (1)$$

$$Y_2 = 3.97 + 2.433X_1 + 1.819X_2 + 2.041X_3 - 0.02264X_1^2 - 0.0599X_1X_2 - 0.1086X_1X_3 \quad (2)$$

ANOVA results of recent regression are reported in Table 2. The calculated Fisher distributions of both models are greater than their critical values. Also, the P-values of them are less than 0.05. Therefore, the compatibility of the models with data is proven. The adjusted determination coefficients of models Y_1 and Y_2 are 91.34% and 96.14%, respectively. So, it can be concluded that no other effective variable has been ignored [33].

Table (2) - ANOVA of the quadratic models of the MDCV biosorption capacity and residual MDCV

Response	Variation source	df	SS	MSS	$F_{calc.}$	F_c	P-value	R^2_{adj}
MDCV biosorption capacity, Y_1	Regression	10	71.07	7.10	28.43	2.49	0.00	91.34%
	Error	16	4.00	0.25	-	-	-	-
	Total	26	75.0778	-	-	-	-	-
Residual MDCV, Y_2	Regression	6	4863.95	810.66	108.85	2.60	0.00	96.14%
	Error	20	148.95	7.45	-	-	-	-
	Total	26	5012.91	-	-	-	-	-

According to Table 3, the P-values of all coefficients of the effective variables in Y_1 analysis is less than 0.05. Since the coefficients of interactions of X_2 and X_4 with other variables are significant, they can not be ignored. Regarding the response of Y_2, all variables except X_4 are significant [33].

Table (3) - Estimated regression coefficients for the quadratic models of the MDCV biosorption capacity and residual MDCV

Terms	Uncoded coefficient		The standard error of the coefficient		t-value		P-value	
	Y_1	Y_2	Y_1	Y_2	Y_1	Y_2	Y_1	Y_2
constant	-5.02	3.97	0.177	0.910	70.03	53.19	0.000	0.000
X_1	0.4863	2.433	0.118	0.643	2.35	-19.43	0.032	0.000
X_2	2.047	1.819	0.118	0.643	1.36	-5.48	0.193	0.000
X_3	0.504	2.041	0.118	0.643	3.88	-10.54	0.001	0.000
X_4	-0.1110	-	0.118	-	-0.33	-	0.744	-
X_1^2	-0.004711	-0.02264	0.274	1.11	-6.88	-8.13	0.000	0.000
X_2^2	-0.1384	-	0.274	-	-4.55	-	0.000	-
X_1X_2	-	-0.0599	-	0.682	-	-5.27	-	0.000
X_1X_3	-0.01156	-0.1086	0.125	0.682	-3.70	-6.37	0.002	0.000
X_1X_4	0.000898	-	0.125	-	2.87	-	0.011	-
X_2X_3	-0.0832	-	0.125	-	-3.99	-	0.001	-
X_3X_4	0.01603	-	0.125	-	5.13	-	0.000	-

Based on Equations 1-2, Y_1 is a second-order function of X_1 and X_2 .Growing of X_3 increases Y_1 and X_4 is almost ineffective. Y_2 increases by enhancement of X_1, X_2, and X_3. Also, X_4 is

completely ineffective. Therefore, it is important to determine the optimal values of variables to maximize the amounts of Y_1 and Y_2 to achieve the maximum biosorption capacity in economic conditions. The optimal values of the recent factors are reported in Table 4. The composite desirability of this optimization is 0.95.

Table (4) - Optimized factors affecting MDCV biosorption capacity and residual MDCV

Optimized factor				Optimized response		Composite desirability
X_1	X_2	X_3	X_4	Y_1	Y_2	
Temperature (°C)	Contact time (hr)	The concentration of phosphoric acid ($mol.L^{-1}$)	The ratio of acid volume to DCV ($mL.g^{-1}$)	MDCV biosorption capacity ($mg.g^{-1}$)	Residual MDCV (%)	
47.3	6.27	2	30	12.61	55.80	0.95

DCV was treated with phosphoric acid under optimized conditions, then it was used as a biosorbent for more experimental results. The experimental data were consistent with the predicted responses. So, optimized MDCV is used in the magnetization stage.

Biosorbent characterization

X-Ray Diffraction (XRD)

The XRD analysis of RCV, DCV, MDCV, and MDCV/Fe_3O_4 are shown in Fig. 1. In the analysis of RCV, the peaks located in the range of 2θ, 23.1, 29.5, 36, 39.5, 43.2, 47.7, 48.6 and 57.5 are attributed to the reflections of (012), (104), (110), (113), (202), (018), (116) and (122) respectively. They represent the magnesium calcite ($(Mg_{0.03}Ca_{0.97})(CO_3)$) with the rhombohedral crystal structure in RCV [34]. It is also found in DCV. The plated distances in these two samples are almost the same [35]. The chart of MDCV has no sharp peaks, so its structure is amorphous. In this diagram, the peaks related to magnesium calcite have been removed. In the analysis of MDCV/Fe_3O_4, peaks in the range of 2θ, 30.1, 35.5, 43.1, 53.5, 57.1 and 62.7 related to reflections (220), (311), (400), (422), (511) and (440) which are shown the presence of iron oxide particles

(Fe_3O_4). Therefore, it can be concluded that the cubic crystal structure of iron oxide is well-formed [32, 36].

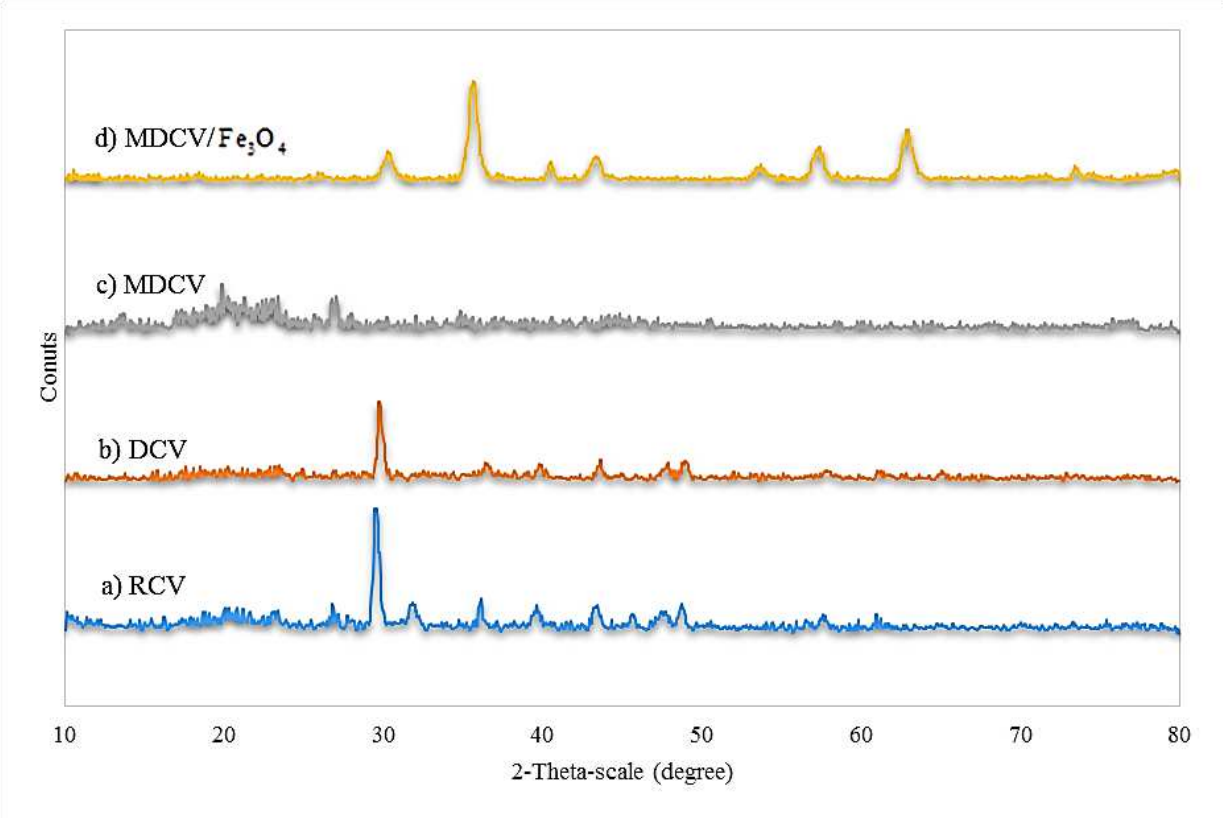

Figure (1) – XRD analysis for a) RCV, b) DCV, c) MDCV and d) MDCV/Fe_3O_4

Fourier Transform Infrared (FTIR)

The results of FTIR analysis for RCV, DCV, MDCV, and MDCV/Fe_3O_4 are shown in Fig. 2. In all samples, the broad peak was observed in the range of 3400 cm^{-1}. It shows the tensile vibrations of the hydroxyl bond (O-H), the amide groups (N-H), and the presence of the water molecules [29]. The peaks around 2926 cm^{-1} are associated with symmetrical and asymmetric tensional vibrations C-H in aliphatic groups such as CH, CH_2, and CH_3 [29]. The intensity of this peak is highest in RCV and almost the same in other samples. In RCV, a peak was observed in 2855 cm^{-1}, indicating CH_2 and CH_3 bonds in fatty acids. It confirms the presence of lipids in the structure of RCV that was removed after the lipid extraction process due to the removal of fatty acids [37]. The peak of 1730 cm^{-1} in RCV indicates tractions in carbonyl ester groups. It was removed by lipid extraction. Then, by acidification and magnetization, two peaks were formed again in the range of

1730 cm^{-1} and 1726 cm^{-1}, which are due to the formation of carboxyl groups. The peaks in the range of 1650 cm^{-1} for all samples are related to the presence of C=O an amide (I) of proteins and the carboxyl functional groups. The peaks in 1549 cm^{-1}, 1540 cm^{-1}, 1537 cm^{-1}, and 1535 cm^{-1} related to RCV, DCV, MDCV and MDCV/Fe_3O_4 respectively, indicate the presence of amide (II) of proteins. Peaks in the region of 1400 cm^{-1} are associated with C-H bonds of lipids and proteins. The peaks in the region of 1260 cm^{-1} are related to C=O bonds in carbonyl amide (II) of proteins and P=O nucleic acid, phosphoryl, and phosphorylate groups .The intensities of these peaks are almost the same in all samples and indicate the preservation of these groups during the process. Also, wide peaks are observed in the range of 1200-900 cm^{-1}, which is related to the C-O-C and C-O bonds present in carbohydrates and polysaccharides [37, 38]. Similar results have been reported by Kristina Maliutina et al. [39]. In RCV and DCV, peaks in 871 cm^{-1} and 875 cm^{-1} are observed respectively, which are related to the presence of CO_3^{2-} mineral compounds such as carbonates. In general, small peaks in the wavelength regions below 600 cm^{-1} are related to the tensile vibrations of organic and mineral halogen compounds such as KCl [40]. About the sample of MDCV/Fe_3O_4, a wide peak is observed in the region of 571 cm^{-1}, which indicates the Fe-O vibrations, so the magnetic property of this sample is confirmed [32].

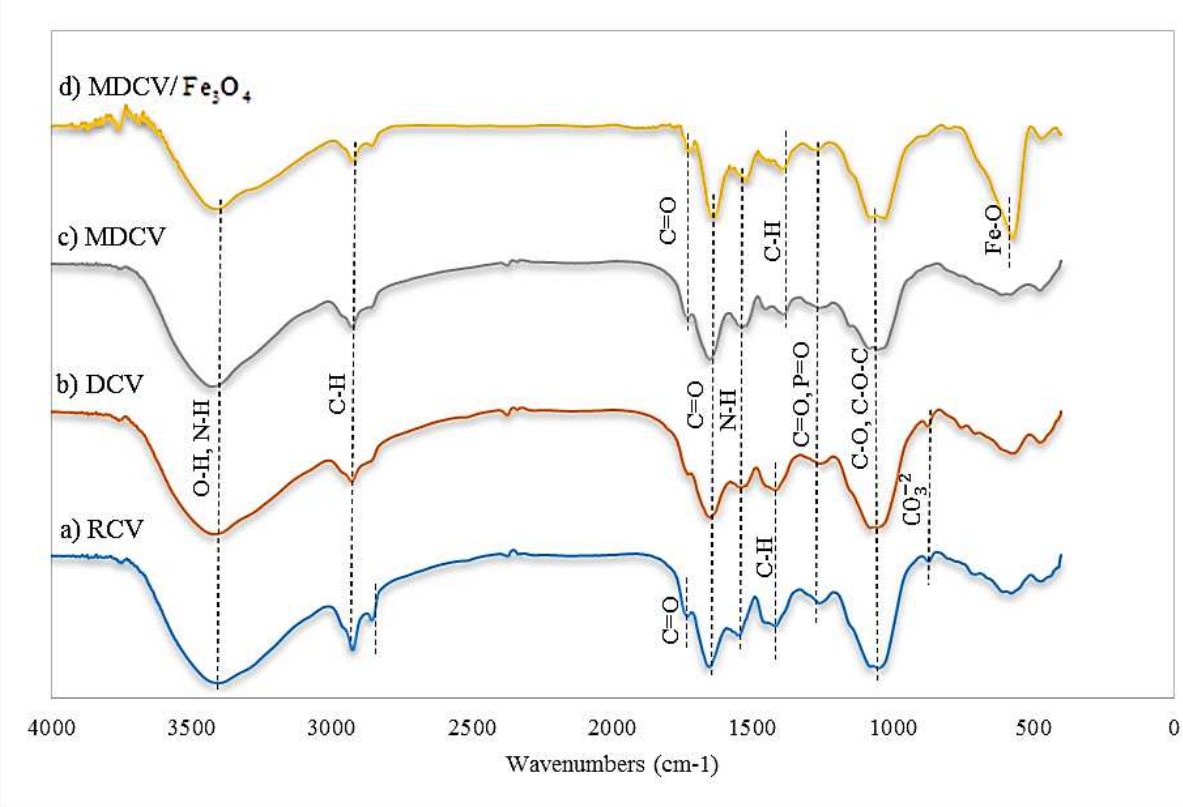

Figure (2) - FT-IR analysis for a) RCV, b) DCV, c) MDCV, and d) MDCV/Fe_3O_4

Scanning Electron Microscopy (SEM)

The results of SEM analysis of RCV, DCV, MDCV, and MDCV/Fe_3O_4 can be seen on the scale of 1 µm and 200 nm in Fig. 3. As shown in Fig. 3a, the crystalline structure of the RCV is heterogeneous. According to Fig. 3b, no significant changes in algae structure occurred after lipid extraction. Chloroform and methanol can enter cell tissue without serious damages to the cell walls [41]. Based on Fig. 3c, phosphoric acid modification has caused severe structural changes. The crystalline structure of DCV has been transformed into an amorphous structure with a uniform and relatively homogeneous surface. Also, the particle size has increased compared to the previous ones. The formation of cavities and bulges on the surface of MDCV is an important factor in increasing the biosorption of dye pollutants [41, 42]. Fig. 3d shows the uniform coverage of the MDCV surface by iron oxide particles and the formation of a spherical crystalline structure [43].

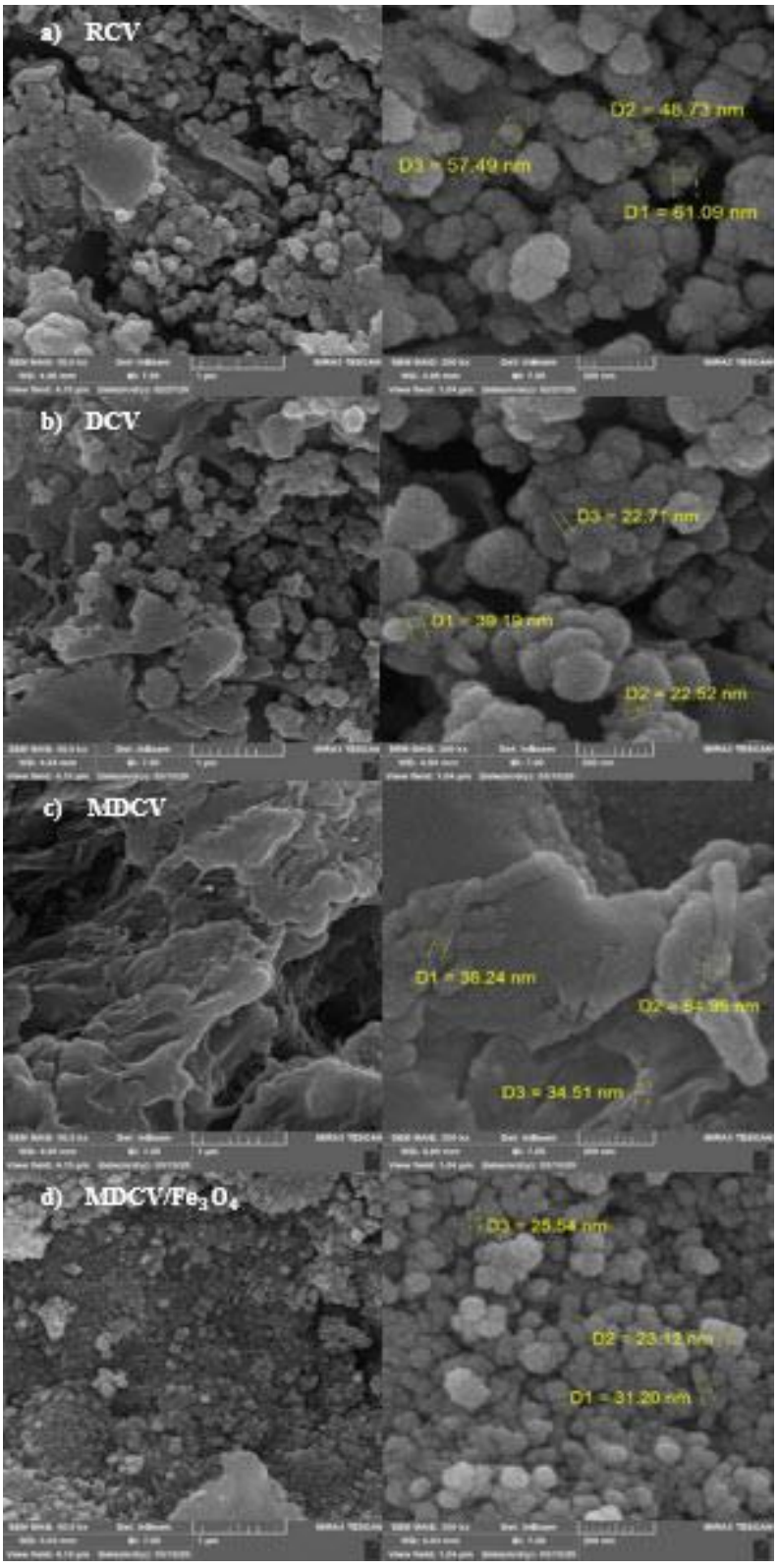

Figure (3) - SEM analysis for a) RCV, b) DCV, c) MDCV, and d) MDCV/Fe_3O_4

Energy-Dispersive X-ray Spectroscopy (EDS)

The EDS analysis was performed to obtain the elements of RCV, DCV, MDCV, and MDCV/Fe_3O_4 that is shown in Fig. 4. Percentages of elements are reported in Table 5. The highest weight percentages in RCV and DCV are related to carbon and oxygen. Other elements such as nitrogen, sodium, magnesium, aluminum, calcium, phosphorus, sulfur, chlorine, potassium, and silicon are also found with a lower weight. According to the results, after magnetization, about 38% of the weight of MDCV/Fe_3O_4 is related to the iron elements. Therefore, the weight ratio of the MDCV: Fe_3O_4 (1:1) is almost confirmed.

Table (5) - Elemental composition of a) RCV, b) DCV, c) MDCV, and d) MDCV/Fe_3O_4

Element	Weight percentage (%)			
	RCV	DCV	MDCV	MDCV/Fe_3O_4
C	40.76	47.1	49.4	18.12
N	10.65	13.38	17.83	7.41
O	34.95	30.43	29.3	35.26
Na	1.14	0.7	1.08	0.21
Mg	0.67	0.65	-	-
Al	0.26	0.31	-	-
Si	1.02	0.54	1.29	0.71
P	1.46	1.4	-	-
S	0.62	0.67	0.53	0.25
Cl	1.04	1.43	0.57	0.19
K	0.63	0.68	-	-
Ca	3.41	2.71	-	-
Ni	3.39	-	-	-
Fe	-	-	-	37.85

Total	100	100	100	100

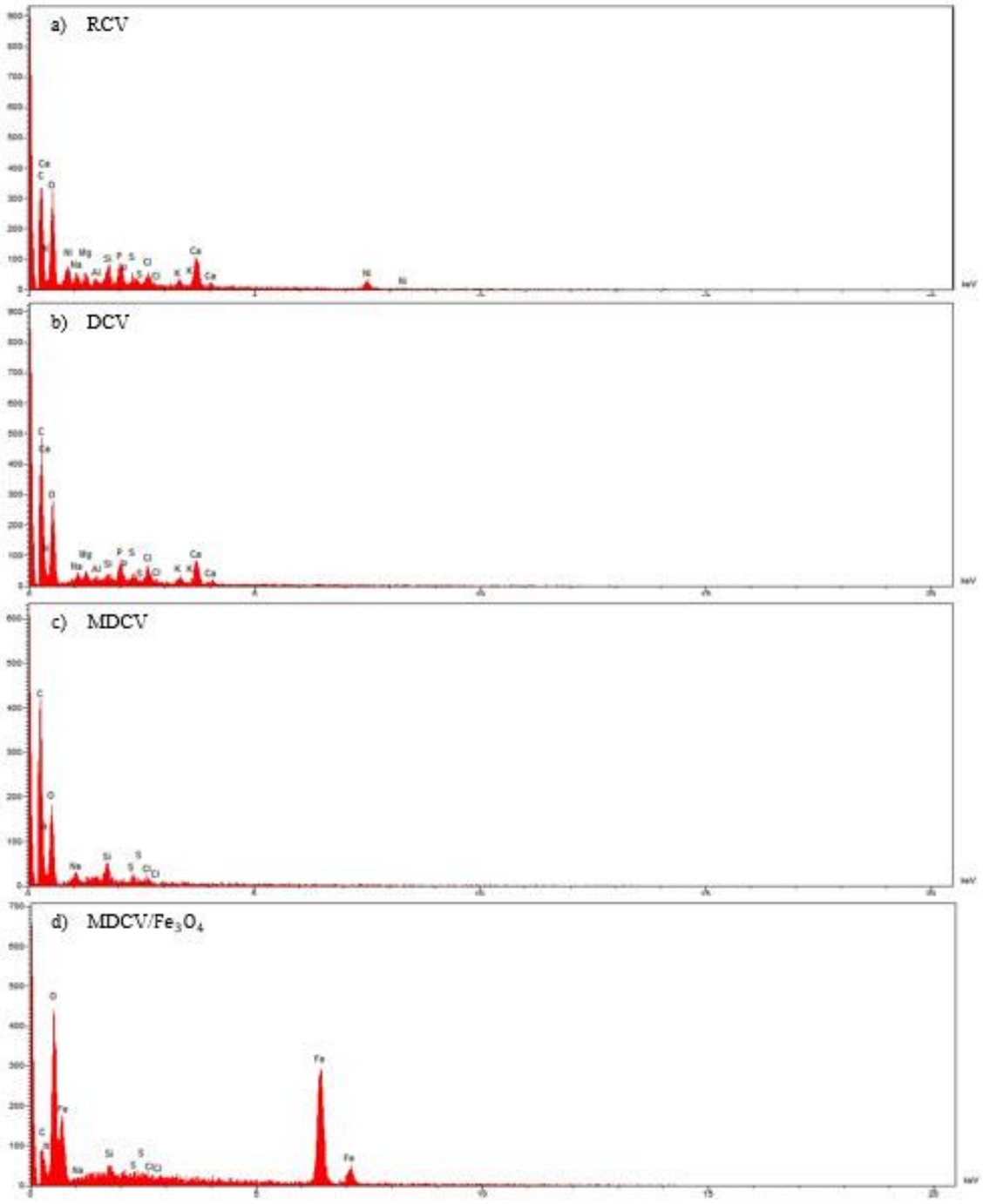

Figure (4) - EDS analysis for a) RCV, b) DCV, c) MDCV, and d) MDCV/Fe_3O_4

Brunauer–Emmett–Teller (BET)

The BET analysis was performed for RCV, DCV, MDCV, and MDCV/Fe_3O_4. Features such as specific surface area, average pore size, and porosity volume of samples were investigated in Table 6. The specific surface area of DCV and MDCV increased about 2 and 15 times, respectively, compared to RCV. The decrement in specific surface area of MDCV/Fe_3O_4 compared to its non-magnetic type was due to the coverage of some of its pores with iron particles. Nevertheless, the specific surface area of MDCV/Fe_3O_4 compared to RCV has increased about 11 times. Thus, the appropriate modification process is confirmed on *Chlorella vulgaris* algae to prepare an easily separable biosorbent while increasing its specific surface area [43]. Fig. 5 shows the nitrogen adsorption-desorption isotherm for the samples. According to the classification of the International Union of Pure and Applied Chemistry (IUPAC), adsorption isotherms are defined in four groups called H1, H2, H3, and H4. The adsorption isotherms of RCV, DCV and MDCV are in H3, and MDCV/Fe_3O_4 is in the H1 category. H1 represents materials with a porous structure that have spherical or cylindrical porous channels. H3 also represents materials with a soft and plate-like structure and porous slits [44, 45].

Based on the Barrett-Joyner-Halenda (BJH) diagram in Fig. 6, the structure of all samples contains micropores, mesopores, and macropores. While the largest distribution of the size of the pores belongs to the group of mesopores with a radius in the range of 2-25 nm [46].

Table (6) - BET analysis results of a) RCV, b) DCV, c) MDCV, and d) MDCV/Fe_3O_4

Sample	Specific surface area (m^2/g)			Average pore size (nm)	Porosity volume (cm^3/g)
	BET	BJH	Langmuir		
RCV	2.30	2.91	2.08	23.84	0.013
DCV	5.27	7.73	3.45	16.21	0.021
MDCV	34.95	36.2	43.89	4.38	0.119
MDCV/Fe_3O_4	25.20	34.12	26.93	13.88	0.087

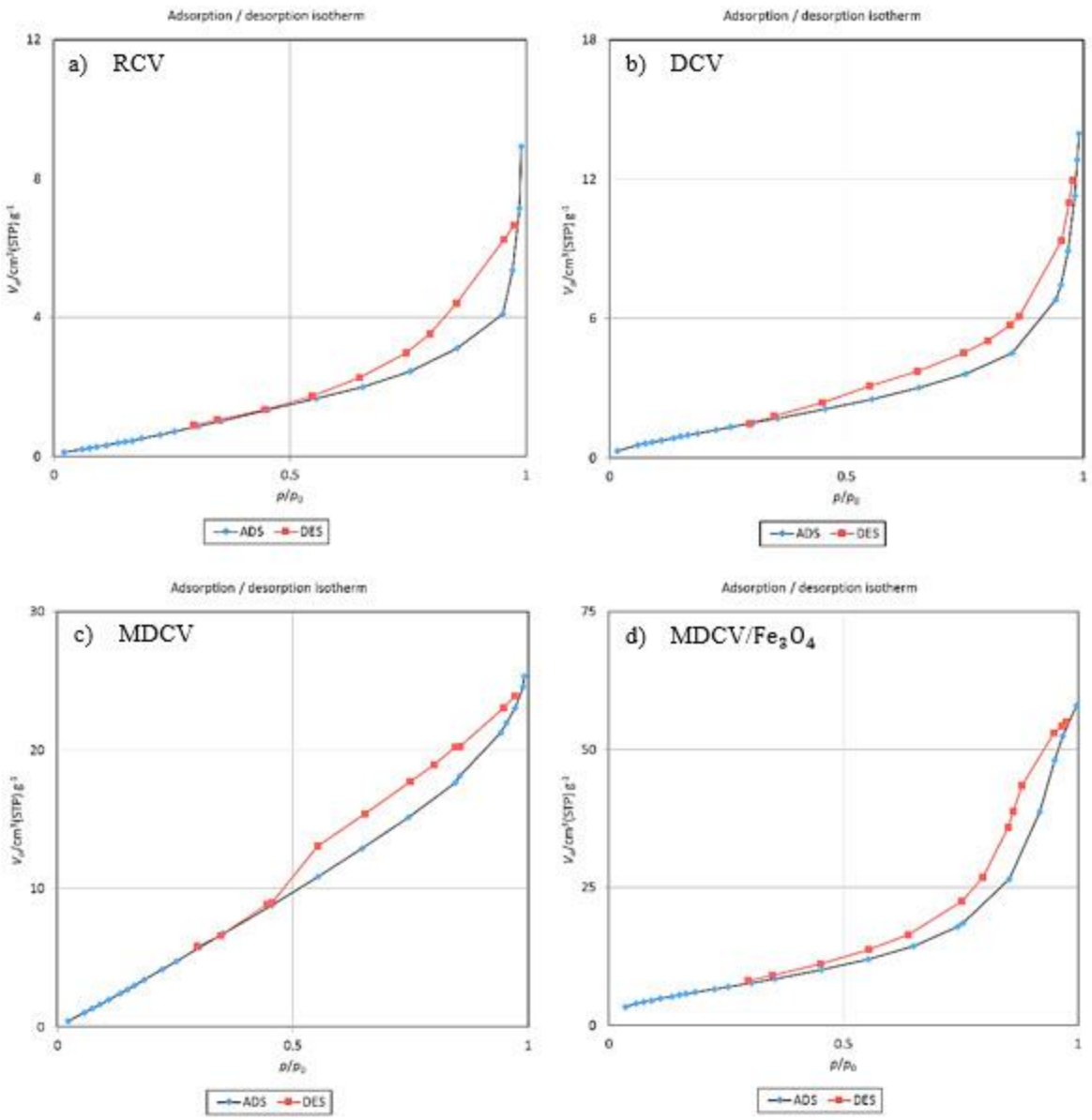

Figure (5) –Nitrogen adsorption-desorption isotherm for a) RCV, b) DCV, c) MDCV, and d) MDCV/Fe_3O_4

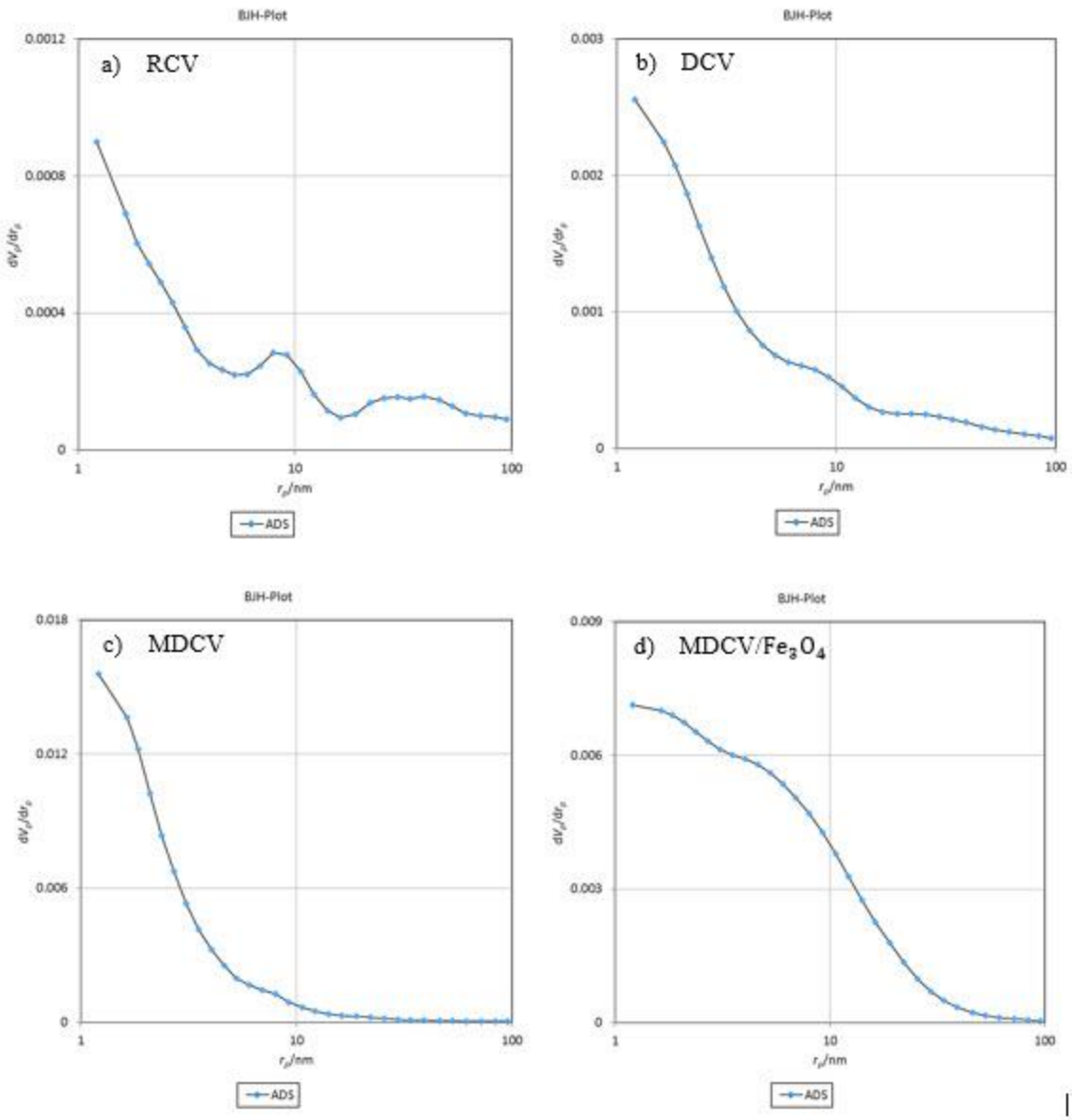

Figure (6) – BJH pore size distribution for a) RCV, b) DCV, c) MDCV, and d) MDCV/Fe_3O_4

Vibrating Sample Magnetometer (VSM)

Based on Fig. 7, the magnetization hysteresis loops of Fe_3O_4 and MDCV/Fe_3O_4 appeared S-like with no remanent magnetization and coercivity. It indicated the strong magnetic response to the different magnetic fields in paramagnetic materials. Therefore, they were easily separable by an external magnetic field and did not stick together when the magnetic field was removed [47]. The saturation magnetization of Fe_3O_4 and MDCV/Fe_3O_4 were 78.64 emu/g and 38.89 emu/g, respectively, which were suitable compared to the magnetic adsorbent derived from *Chlorella*

vulgaris reported by M. Govarthanan [48]. The decrease in MDCV/Fe_3O_4 magnetization relative to Fe_3O_4 was due to changes in particle size, irregular bonding of particles, and surface spin disorientation [49, 50].

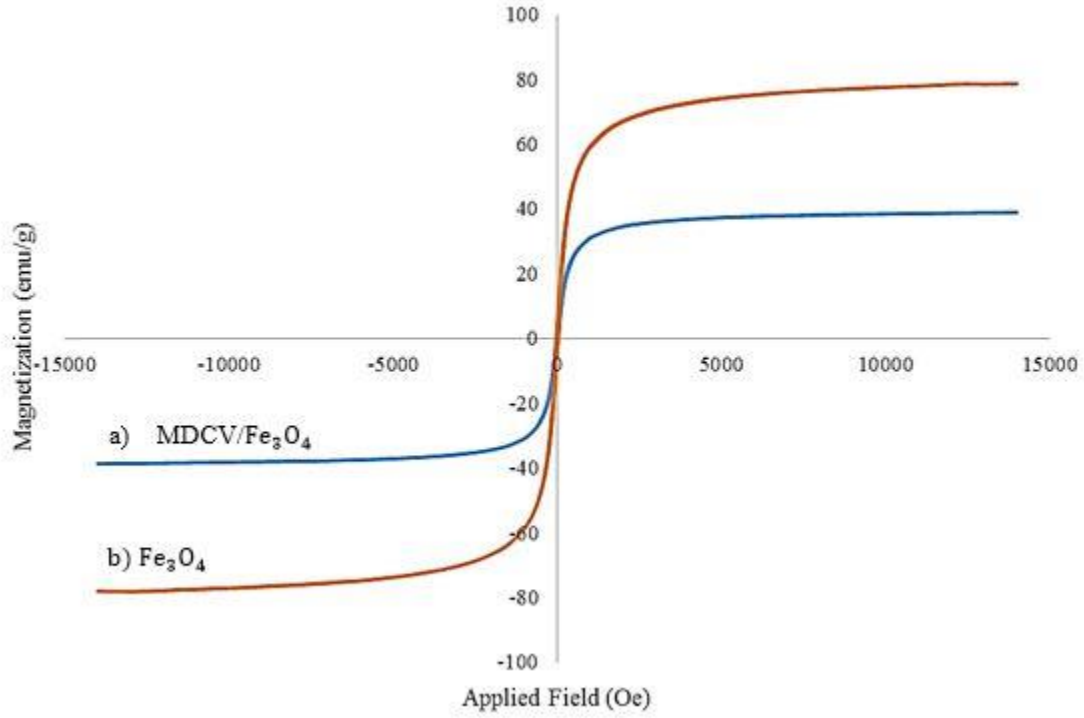

Figure (7) – VSM analysis for a) MDCV/Fe_3O_4, b) Fe_3O_4

Biosorption analysis

Experimental results for biosorption analysis are reported in Table 7. Based on Equation 3, the multiple regression analysis of experimental data with 95% probability was used to study the effect of each parameter on the biosorption capacity of MDCV/Fe_3O_4, kinetics, isotherms, and thermodynamic models. Ineffective variables were removed to increase the suitability of the models with experimental data.

Table (7) - Experimental results of biosorption analysis from CCD proposed levels

Run no.	X_1, T	X_2, t	X_3, m	X_4, C_0	X_5, pH	Y, q_{MDCV/Fe_3O_4}
1	-1	-1	-1	-1	1	10.7565
2	1	-1	-1	-1	-1	7.8790
3	-1	1	-1	-1	-1	8.7164
4	1	1	-1	-1	1	8.8619
5	-1	-1	1	-1	-1	3.8118
6	1	-1	1	-1	1	3.6523
7	-1	1	1	-1	1	4.0791
8	1	1	1	-1	-1	3.4669
9	-1	-1	-1	1	-1	23.1100
10	1	-1	-1	1	1	27.4232
11	-1	1	-1	1	1	26.2010
12	1	1	-1	1	-1	25.9489
13	-1	-1	1	1	1	13.4475
14	1	-1	1	1	-1	12.5616
15	-1	1	1	1	-1	11.5723
16	1	1	1	1	1	13.3958
17	-1	0	0	0	0	11.3094
18	1	0	0	0	0	9.3598
19	0	-1	0	0	0	12.7255
20	0	1	0	0	0	12.3278

21	0	0	-1	0	0	13.2300
22	0	0	1	0	0	6.0006
23	0	0	0	-1	0	6.1024
24	0	0	0	1	0	18.6266
25	0	0	0	0	-1	8.5650
26	0	0	0	0	1	9.3695
27	0	0	0	0	0	11.5809
28	0	0	0	0	0	11.5809
29	0	0	0	0	0	10.2133

$$Y = -3.72 - 0.0411X_1 - 0.2702X_2 - 0.1062X_3 + 0.0994X_4 + 5.72X_5 + 0.002240X_2^2 + 0.001158X_4^2 - 0.386X_5^2 + 0.000664X_1X_4 - 0.003177X_3X_4 \quad (3)$$

The compatibility of the models with data is proven by the ANOVA results of recent regression. Based on Table 8, the calculated Fisher distributions is greater than its critical value. Also, the P-value is less than 0.000. The adjusted determination coefficient of model Y is 98.35% [51].

Table (8) - ANOVA of the quadratic models of the MDCV/Fe_3O_4 biosorption capacity

Response	Variation source	df	SS	MSS	$F_{calc.}$	F_c	P-value	R^2_{adj}
MDCV/Fe_3O_4 biosorption capacity, Y	Regression	10	1207.00	120.70	168.20	2.19	0.00	98.35%
	Error	18	12.92	0.718	-	-	-	-
	Total	28	1219.92	-	-	-	-	-

According to Table 9, the P-values of all coefficients of the effective variables in Y analysis are less than 0.05. Since the coefficients of interactions of X_2^2 and X_1X_4 are significant, X_1 and X_2 can not be ignored [51].

Table (9) - Estimated regression coefficients for the quadratic model of the MDCV/Fe_3O_4 biosorption capacity

Terms	Uncoded coefficient	The standard error of the coefficient	t-value	P-value
constant	-3.72	0.274	38.26	0.000
X_1	-0.0411	0.200	-0.13	0.901
X_2	-0.2702	0.200	-0.22	0.827
X_3	-0.1062	0.200	-22.30	0.000
X_4	0.0994	0.200	31.99	0.000
X_5	5.72	0.200	3.22	0.005
X_2^2	0.002240	0.504	4.00	0.001
X_4^2	0.001158	0.504	3.68	0.002
X_5^2	-0.386	0.504	-3.06	0.007
X_1X_4	0.000664	0.212	2.51	0.022
X_3X_4	-0.003177	0.212	-9.00	0.000

Effect of contact time

The biosorption capacity of MDCV/Fe_3O_4 was plotted in Fig. 8a. The biosorption capacity is zero at the beginning of the process. It reaches the maximum levels during the first five minutes. Then, it decreases over time and reaches equilibrium mode. This phenomenon is called repulsion. It occurs when large biosorption surface areas are available and rapidly covered by MB molecules in the first few minutes [52-54]. Eventually, the system reaches equilibrium after a while of biosorption and desorption. In the first minutes, the higher MB concentration, due to the high driving forces of mass transfer, increase the biosorption capacity. So the highest MB removal efficiency appears in the first minutes before the time of equilibrium. After reaching equilibrium, the removal efficiency of MB by MDCV/Fe_3O_4 at initial concentrations of 20, 60, and 100 mg/L are about 63%, 37% and 37%, respectively.

Effect of pH

The pH of the solution significantly affects the relationship between biosorbent and adsorbate. On the other hand, the interactions of hydrogen ions, Van der Waals forces, and the propagation of cavities, also affect the biosorption rate. As can be seen in Fig. 8b, the amounts of biosorption capacity in pH 3 to 7 increased from 17.6 to 25 mg/g and then it decreased to 13 mg/g as the pH increased to 9. The cell wall of *Chlorella vulgaris* contains a large number of functional groups, carboxylic acid. Therefore, at low pH, cell wall ligands are protonated and the H^+ also increases. As a result, the biosorption capacity decreased due to the competition between H^+ and cationic molecules of MB. As the pH increased and OH^- formed, more ligands, such as the amino and carboxyl functional groups, were exposed to the attraction between OH^- and MB cationic molecules. The competition between H^+ and MB also decreased, so the biosorption capacity of MDCV/Fe_3O_4 increased [55, 56]. At higher pHs, the presence of ions, MB cationic molecules, and the interactions of charges increased the forces between MB monomer molecules. This phenomenon had led to the formation of MB dimer molecules, which were probably larger than the size of surface holes. This difference in sizes reduced the number of active surface cavities and caused less biosorption capacity [57].

Effect of biosorbent dosage

Based on Fig. 8c, the development of biosorbent amount increases the removal efficiency of MB due to the increment of active sites for dye biosorption. While the reduction in biosorption capacity by increasing the amount of biosorbent is due to the gradient of the biosorbent and adsorbate concentration. The factors influencing biosorption are investigated based on the biosorbent mass unit. As a result, phenomena such as aggregation and condensation cause many active levels to remain unused, thereby reducing biosorption capacity. It is observed that the biosorption capacity and removal efficiency of MB in the biosorbent amounts of 15 to 45 mg has changed from 25 mg/g and 37% to 12 mg/g and 55%, respectively [58, 59].

Effect of the initial concentration of MB

Changes in the biosorption capacity and removal efficiency of MB are calculated according to the changes in the initial concentration of MB and reported in Fig. 8d. By changing the initial concentration of MB from 20 to 100 mg/L, the biosorption capacity has increased from 8.5 to 25

mg/g, due to mass transfer-driving forces. As mentioned in the previous section, the removal efficiency of MB is directly related to the number of active sites of the biosorbent. Therefore, at a constant biosorbent dosage, with increasing the initial concentration of MB, the active sites of the biosorbent decrease and lead to the reduction in removal efficiency from 63% to 37% [60].

Effect of temperature

As mentioned in the ANOVA analysis section, the temperature does not significantly affect the MDCV/Fe_3O_4 biosorption capacity. According to Fig. 8e, with increasing temperature from 5 to 45℃, the biosorption capacity of MDCV/Fe_3O_4 with initial MB concentration of 60 mg/L did not change much and with initial MB concentrations of 20 mg/L and 100 mg/L was associated with a decrease of 12% and an increase of 4%, respectively. Similar results were observed in recent research by Konig-Peter Aniko et al. [61]. These differences in the behavior of MDCV/Fe_3O_4 biosorption capacity relative to temperature indicates that the biosorption process is entropically rather than enthalpically driven [62].

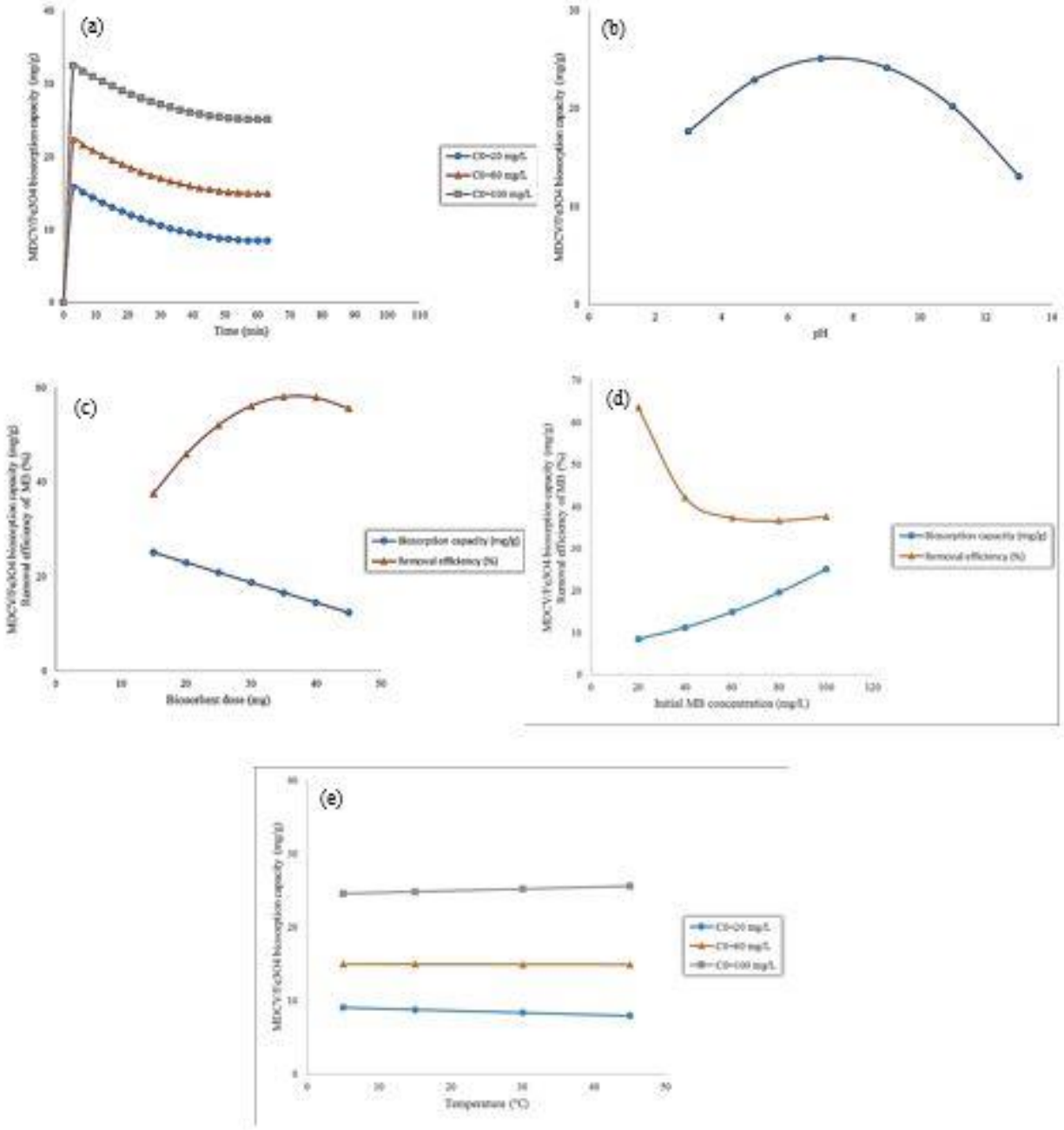

Figure (8) - Effect of a) contact time (T=25℃, m=15 mg, pH=7), b) pH (T=25℃, t=60 min, m=15 mg, C0=100 mg/L), c) biosorbent dosage (T=25℃, t= 60 min, C0=100 mg/L, pH=7), d) initial concentration of MB (T=25℃, t=60 min, m=15 mg, pH=7), and e) temperature (t= 60 min, m=15 mg, pH=7) on biosorption of MB by MDCV/Fe_3O_4

Biosorption kinetics

Kinetic trends and their parameters are reported in Fig. 9 and Table 10. Due to the downward trend in biosorption capacity over time, the pseudo-first-order model cannot be examined [63]. The determination coefficients of the pseudo-second-order model in all initial concentrations of MB are greater than 0.99. Also, the equilibrium biosorption capacities calculated in this model are very close to the experimental amounts. Therefore, this model is a good predictor of the kinetics of MB biosorption on the MDCV/Fe_3O_4 and more compatible than the intraparticle diffusion model [63]. Based on the intraparticle diffusion model, increasing the value of surface biosorption (intercept, C) with increasing temperature indicates a decrease in the rate of diffusion of MB from the external surface to the internal surfaces of biosorbent [64].

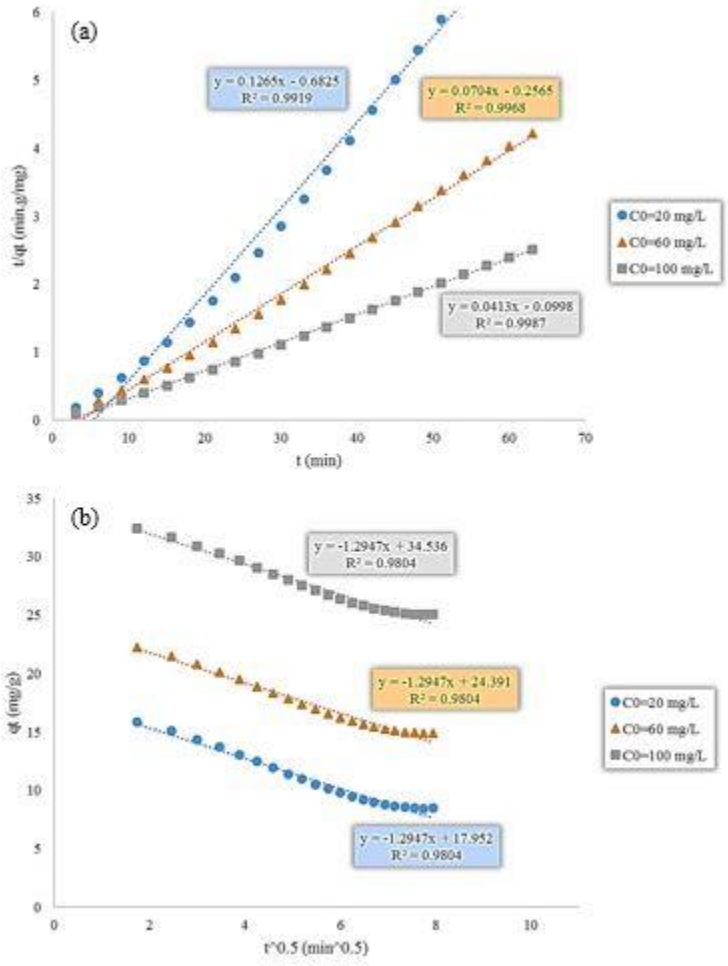

Figure (9) - Plots of a) pseudo-second-order, b) intraparticle diffusion kinetic models for MB biosorption onto MDCV/Fe_3O_4 (T=25℃, m=15mg, pH=7)

Table (10) - Kinetic parameters for MB biosorption onto MDCV/Fe_3O_4

Parameter	Concentration (mg/L)		
	20	60	100
$q_{e,exp}$ $(mg.g^{-1})$	8.46	14.90	25.05
t_e (min)	60	60	60
Pseudo-second-order			
$q_{e,cal}$ $(mg.g^{-1})$	7.90	14.20	24.21
k_2 $(g.mg^{-1}.min^{-1})$	-0.0234	-0.0193	-0.0170
R^2	0.99	0.99	0.99
Intraparticle diffusion			
k_{id} $(mg.g^{-1}.min^{0.5})$	-1.2947	-1.2947	-1.2947
C $(mg.g^{-1})$	17.952	24.391	34.536
R^2	0.98	0.98	0.98

Biosorption isotherms

Comparing the results of Fig. 10 and Table 11, Freundlich isotherm has the highest compatibility with data compared to Langmuir and Temkin. The equilibrium parameters of the Langmuir isotherm (R_L) are in the range of $0 < R_L < 1$. Also, in the Freundlich isotherm, the values of 1/n are in the range of $0 < 1/n < 1$. So, the biosorption of MB onto MDCV/Fe_3O_4 is desirable [65, 66]. The values of K_f also indicate a growth in biosorption capacity with decreasing temperature. The decreasing of b_t with increasing temperature in Temkin isotherm, indicates an exothermic biosorption [67].

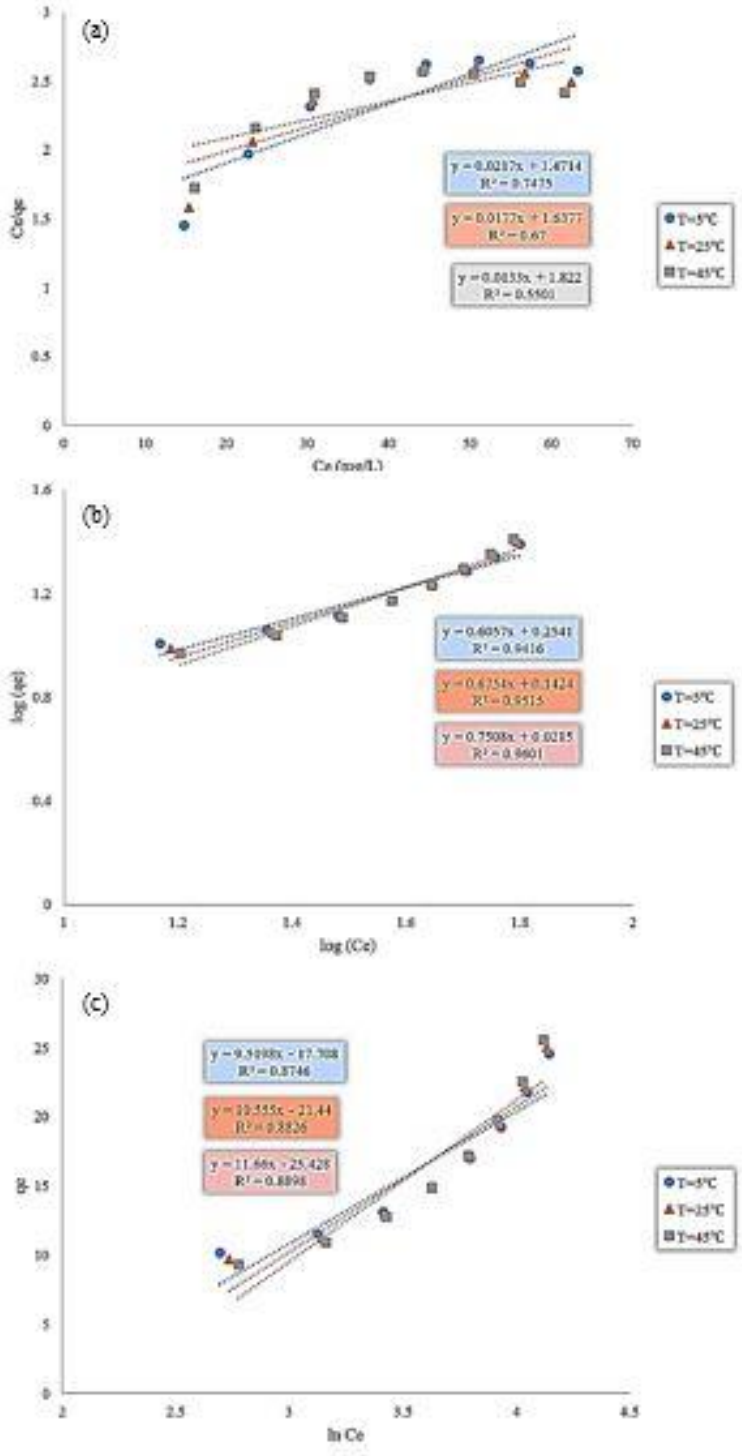
(a)
Ce/qe
Ce (mg/L)
y = 0.0287x + 1.4714
R² = 0.7475
y = 0.0177x + 1.6377
R² = 0.67
y = 0.0133x + 1.822
R² = 0.5501
T=5°C
T=25°C
T=45°C
(b)
log (qe)
log (Ce)
y = 0.6057x + 0.2541
R² = 0.9416
y = 0.6754x + 0.1424
R² = 0.9515
y = 0.7508x + 0.0285
R² = 0.9601
T=5°C
T=25°C
T=45°C
(c)
qe
ln Ce
y = 9.5108x - 17.708
R² = 0.8746
y = 10.555x - 23.44
R² = 0.8826
y = 11.66x - 25.428
R² = 0.8998
T=5°C
T=25°C
T=45°C

a

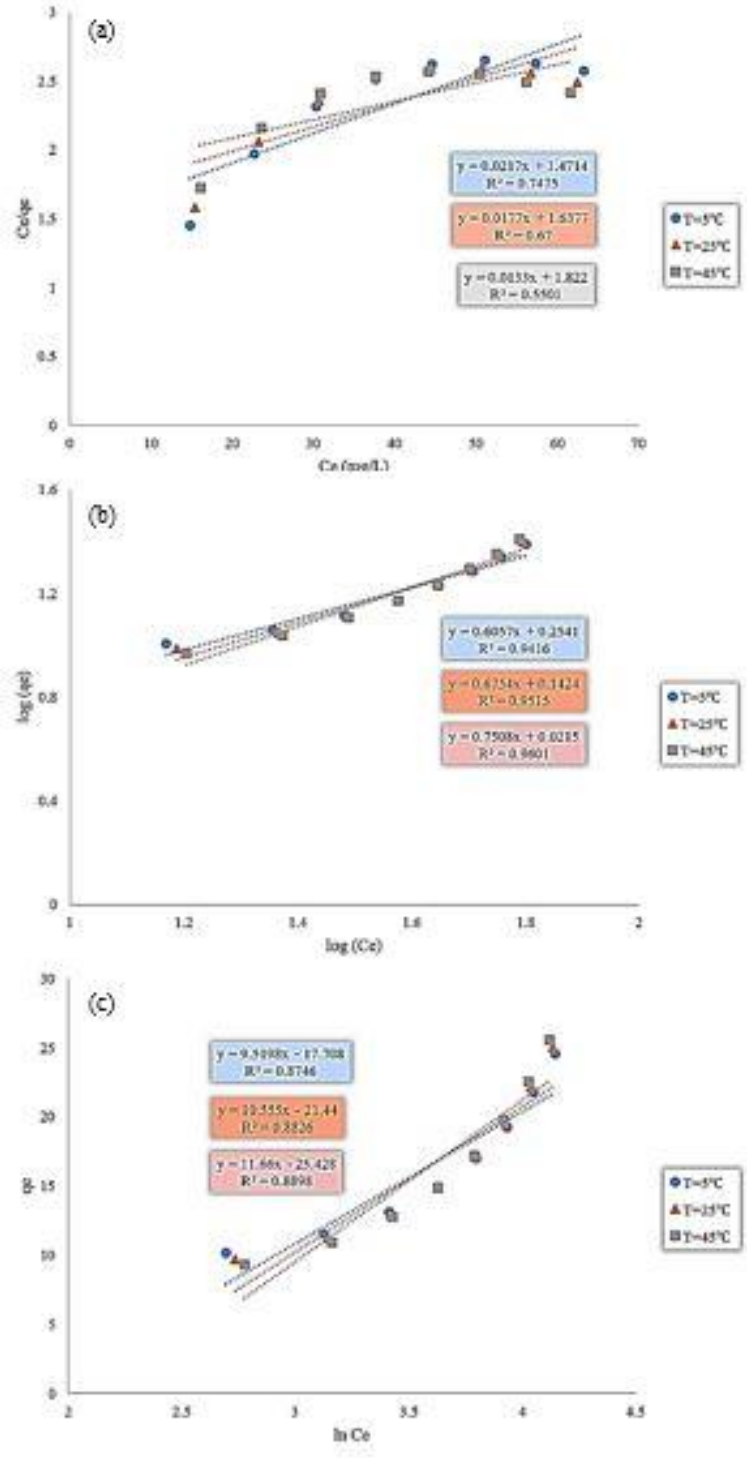

Figure (10) - Plots of a) Langmuir, b) Freundlich, c) Temkin isotherm models for MB biosorption onto MDCV/Fe_3O_4

Table (11) - Isotherm parameters for MB biosorption onto MDCV/Fe_3O_4

Parameter	Temperature (℃)		
	5	25	45
Langmuir			
K_L $(L.mg^{-1})$	0.014	0.010	0.007
q_m $(mg.g^{-1})$	46.08	56.50	75.18
R_L	0.40-0.69	0.48-0.75	0.58-0.82
R^2	0.74	0.67	0.55
Freundlich			
K_F $((mg.g^{-1})(mg.L^{-1})^{1/n})$	1.79	1.38	1.05
n	1.65	1.48	1.33
R^2	0.94	0.95	0.96
Temkin			
b_t $(J.g.mol^{-1}.mg^{-1})$	242.78	234.72	226.74
K_T $(L.mg^{-1})$	0.15	0.13	0.11
R^2	0.87	0.88	0.88

Biosorption thermodynamic

The Van't Hoff plot of $ln\,K_c$ versus $1/T$ is shown in Fig. 11. The calculated thermodynamic parameters are reported in Table 12. Positive values of ΔG indicate the non-spontaneous biosorption of MB onto MDCV/Fe_3O_4, which grows with increasing temperature [50]. The result of changes in the energy of the biosorption and desorption has led to a negative amount of ΔH. As a result, the biosorption process of MB on MDCV/Fe_3O_4 is exothermic [68]. Based on previous studies and considering the enthalpy value (-46.56 kJ/mol), the biosorption process of MB onto MDCV/Fe_3O_4, is considered as almost physical biosorption [69, 70]. The negative value of ΔS

also indicates a reduction in randomness and irregularity of MB particles when they are placed on the active sites of biosorbent [71].

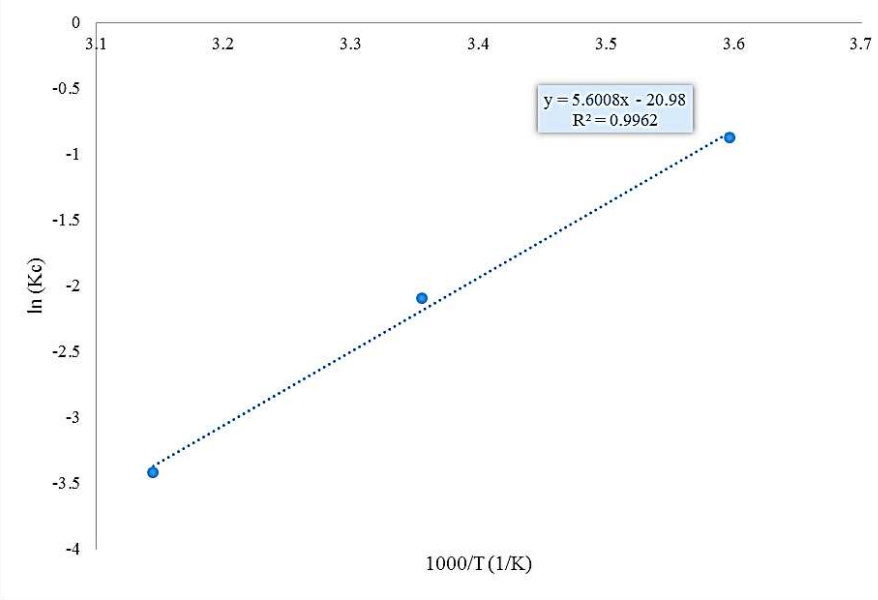

Figure (11) - Van't Hoff diagram for the estimation of thermodynamic parameters

Table (12) – Thermodynamic parameters for MB biosorption onto MDCV/Fe_3O_4

Parameter	Temperature (K)			R^2
	278	298	318	
K_c	0.4167	0.1230	0.0328	0.99
$\Delta H\ (kJ.mol^{-1})$		-46.56		
$\Delta S\ (kJ.mol^{-1}.K^{-1})$		-0.17		
$\Delta G\ (kJ.mol^{-1})$	1.92	5.41	8.90	

Comparison of MDCV/Fe_3O_4 with other biosorbents

The maximum biosorption capacity of the biosorbents depends on the modification method and the type of dyes. The maximum biosorption capacity of MDCV/Fe_3O_4 is 32.44 mg/g at temperature (45℃), contact time (5 min), biosorbent dosage (15 mg), initial concentration of MB (100 mg/L), and pH (7). Comparison of MDCV/Fe_3O_4 with other biosorbents for MB biosorption was

performed in Table 13. The results show that the maximum biosorption capacity of MDCV/Fe_3O_4 is good. Although this amount is lower than some biosorbents such as biochars and their activated carbons, it is promising and even higher compared to some green, red, and brown algae with similar modifications. On the other hand, few studies have been done on the modified dry *Chlorella vulgaris*. Therefore, this study offers a useful approach in MB biosorption with maximum removal efficiency during the shortest time.

Table (13) - Comparison of MDCV/Fe_3O_4 maximum biosorption capacity ($q_m, mg/g$) with other biosorbents

Biosorbent	Modification	Maximum biosorption capacity (mg/g)	Ref.
Enteromorpha spp.	-	274	[72]
Nizamuddinia zanardinii	-	863.4	[73]
Magnetic *wakame* biochar nanocomposites	Magnetization Loading nickel on biochar	479.49	[74]
Ultrasonicated activated carbon of empty fruit bunch	Ultrasonication	435	[71]
Activated carbon of Empty Fruit Bunch	-	400	[71]
Aegagropila Linnaei	-	250	[75]
Chemical modified *Aegagropila Linnaei*	Extracted functionalized cellulose	100	[75]
EDTA-modified bentonite	Modification with EDTA	160	[76]
Gracilaria parvispora	-	83.08	[73]
Palm leaflets	-	72.3	[77]
Palm frond base	-	70.87	[77]
Cystoseira barbatula	-	38.61	[78]
Raw wet *Chlorella vulgaris*	-	10.142	[79]

Annona squmosa seed	Sulfuric acid activation	8.52	[80]
S. dimorphus	-	6	[81]
Defatted algal biomass of *S.dimorphus* (DAB)	Lipid extraction	7.73	[81]
Sulfuric acid pretreated DAB	Sulfuric acid pretreatment	7.80	[81]
Raw *posidonia oceanica* fibres	-	5.56	[82]
Caulerpa racemosa var. *cylindracea*	-	5.23	[83]
This work	Lipid extraction Phosphoric acid modification Magnetization	32.44	-

Conclusion

In this work, *Chlorella vulgaris* algae was examined to remove MB from wastewater. This study showed that lipid extraction could provide a good opportunity to use algae residues after the esterification process as an economic biosorbent. Optimization of the variables in the phosphoric acid modification process ensured the maximization of the biosorption capacity and residual defatted algae. Finally, the modified defatted algae were magnetized for easy and low-cost separation of the biosorbent. The specific surface area of the magnetic modified defatted algae (MDCV/Fe_3O_4) reached 25.2 m^2/g .So a novel magnetic biosorbent was considered to remove MB. Parameters affecting the biosorption were investigated to increase the biosorption capacity of MDCV/Fe_3O_4. The pseudo-second-order kinetic model was well matched to the data. Equilibrium data were well described by the Freundlich model. MB biosorption on the selected biosorbent was non-spontaneous and exothermic. This process was associated with decreasing irregularity and randomness at the interface of dye and biosorbent. This study proved that *Chlorella vulgaris* can be used as a cheap and available source to remove the MB dye pollutant.

Methods

Materials

Chlorella vulgaris algae were obtained from the Biotechnology Laboratory, Faculty of Chemical Engineering, University of Tehran, Tehran, Iran. Chloroform ($CHCl_3$, 98%), methanol (CH_3OH, 99.5%), ortho-phosphoric acid (H_3PO_4, 85%) and sodium carbonate anhydrous (Na_2CO_3, 99.9%) were purchased for extraction of lipids and acid treatment from Merck. For magnetization, iron (II) sulfate heptahydrate ($FeSO_4.7H_2O$, 99%), iron (III) chloride hexahydrate ($FeCl_3.6H_2O$, 99%), and ammonia (NH_4OH, 25wt%) was purchased from Merck. Methylene blue Powder ($C_{16}H_{18}ClN_3S$, ≥82%), sodium hydroxide ($NaOH$, 98%), and hydrochloric acid (HCl, 37%) were purchased from Merck for the biosorption process. All chemicals are in the analytical grade.

Biosorbent preparation

Raw *Chlorella vulgaris* algae (RCV) was first washed several times with distilled water to remove impurities and dried at 45℃ for 24 hr. Then it was powdered with mortar.

Lipid extraction

Lipid extraction of RCV was performed by ultrasonic cell destruction and Soxhlet extraction setup [84]. First, 10 g of RCV was mixed with 10 mL of methanol. Then it was sonicated with the frequency of 28 kHz at room temperature for 40 minutes. The sonicated RCV was then transferred to a cartridge and placed inside the Soxhlet setup. As a solvent mixture, 285 mL of chloroform:methanol (1:2 v/v) was poured into the flask according to Bligh & Dyer method [85]. Extraction was carried out for 24 hr at 65℃. The defatted *Chlorella vulgaris* (DCV) was washed several times with distilled water to remove the remaining solvent and dried at 50℃ for 24 hr. Dry DCV was powdered with a mortar and used for the next steps.

Phosphoric acid treatment and optimization of parameters

DCV was exposed to a dilute phosphoric acid solution under specified conditions. The central composite design (CCD) was used by the response surface methodology (RSM) to design experiments. Coded & uncoded levels of variables such as the reaction temperature (X_1), the contact time (X_2), the concentration of phosphoric acid (X_3), the ratio of acid solution volume to

DCV (X_4), MDCV biosorption capacity (Y_1), and residual MDCV(Y_2), determined by the design of experiments, are shown in Table 14. The number of 27 experiments including 8 axial points (α = 1) and 3 central points were considered in CCD. About 0.1 g of DCV was treated under each designed experimental conditions. Finally, MDCV was filtered and neutralized with deionized water and 0.1 M sodium carbonate. It was then dried at 50℃ for 24 hr and crushed into fine particles. The MDCV biosorption capacities and the residual MDCV were considered as experimental design responses. The residual of MDCV was calculated using Equation 4:

$$Residual\ MDCV\ (\%) = \frac{m_2}{m_1} \times 100 \quad (4)$$

Where m_1 and m_2 are the mass of DCV (mg) before and after acid treatment, respectively.

Table (14) - Levels of coded and uncoded variables for the MDCV biosorption capacity and residual MDCV

Variable	Name	Range of levels		
		-1	0	1
X_1	The temperature of the reaction, T, ℃	30	50	70
X_2	The contact time of DCV with acid, t, hr	3	6	9
X_3	The concentration of acid, C_A, mol/L	2	4	6
X_4	The ratio of acid volume to DCV, V/W, mL/g	30	50	70
Y_1	MDCV biosorption capacity, q_{MDCV}, mg/g			
Y_2	Residual MDCV, RP_{MDCV}, %			

Considering the last responses, the regression, and the variance analysis (ANOVA) were done using Minitab-18 software. Optimal conditions were calculated in the maximum amount of both responses and DCV was modified in those conditions [33].

MDCV/Fe_3O_4 preparation

Synthesis of MDCV/Fe_3O_4 particles were performed by the co-precipitation method [86, 87]. To do that, about 0.1 g of MCDV was stirred with 100 mL of deionized water for 5 minutes and then sonicated with the frequency of 28 kHz at room temperature for 30 minutes. Sonicated solution was added to 100 mL of an aqueous solution containing $FeSO_4.7H_2O$ and $FeCl_3.6H_2O$ with a 1:2 M ratio. The mixture was stirred under a nitrogen atmosphere at 85℃ and 250 rpm. After 15

minutes, about 10 mL of ammonia was added dropwise to the system for setting the pH about 9. The reaction continued for an hour. The MDCV/Fe_3O_4 particles were separated using an external magnet and washed several times with deionized water to reach pH 7. Finally, MDCV/Fe_3O_4 particles were dried at 50℃ for 24 hr and then powdered by mortar [32, 88].

Biosorption analysis

The biosorption of MB on MDCV/Fe_3O_4 was performed in a batch using an incubator at 200 rpm. The effect of variables such as temperature (X_1), contact time (X_2), biosorbent dosage (X_3), initial concentration of MB (X_4), and pH (X_5) were investigated. NaOH and HCl 0.1M were used to regulate the pH. The experiments were performed using the CCD by RSM involving 29 runs with 3 central points and 10 axial points ($\alpha = 1$). The coded and uncoded conditions specified by the experimental design are shown in Table 15.

Table (15) - Levels of coded and uncoded biosorption variables using MDCV/Fe_3O_4 as a biosorbent

Variable	Name	Range of levels		
		-1	0	1
X_1	Temperature, T, ℃	5	25	45
X_2	Contact time, t, min	30	60	90
X_3	Biosorbent dosage, m, mg	15	30	45
X_4	Initial concentration of MB, C_0, mg/L	20	60	100
X_5	pH	5	7	9
Y	biosorption capacity of MDCV/Fe_3O_4, q_{MDCV/Fe_3O_4}, mg/L			

The final concentration of MB was obtained using a UV-Visible spectrophotometer at λ_{max} =665 nm [89]. Biosorption capacity (mg/g) and removal percentage (%) were calculated based on the following Equations:

$$q_t = \frac{(C_0 - C_t) \times V}{m} \quad (5)$$

$$R = \frac{(C_0 - C_t) \times 100}{C_0} \quad (6)$$

Where C_0 and C_t are the initial and final concentrations of MB (mg/L), respectively. V is the volume of the dye pollutant (L) and m is the biosorbent dosage (g).

Regression, and variance analysis (ANOVA) of the biosorption capacity of MDCV/Fe_3O_4 were done using Minitab-18 software.

Statistical analysis

The design of the experiments was done by using the central compound design (CCD) of the response surface methodology (RSM). The responses were considered based on the quadratic functions with the interaction of the variables affecting them according to Equation 7. Also, the levels of variables are based on Equation 8 [90].

$$y = \beta_0 + \sum_{i=1}^{k} \beta_i x_i + \sum_{i=1}^{k} \beta_{ii} x_i^2 + \sum_{1 \le i \le j}^{k} \beta_{ij} x_i x_j + \varepsilon \quad (7)$$

$$x_i = \left(\frac{z_i - z_i^0}{\Delta z_i}\right) \beta_d \quad (8)$$

Where β_i shows the coefficients of the parameters of the quadratic function, z_i and x_i are real and coded values, respectively. Δz_i is the distance between the value of the center point and the next or previous levels. β_d is the major coded value for each variable. z_i^0 is the real value of the center point.

The relation between the total sum of the square (SS_{Total}), the sum of the square due to regression (SS_{Reg}), and errors (SS_{Error}) is based on Equation 9. The equations for calculating the sum of squares and the mean sum of squares of the data are shown in Table 16. The matching of the regression model and experimental data is determined by using the calculated Fisher distribution ($F_{calc.}$), the critical Fisher distribution (F_c), the probability value (P-value), and the adjusted determination coefficient ($R^2_{adj.}$), as shown in Equations 10-13 [90]. The statistical calculations are also based on the probability of 95% ($\alpha = 0.05$).

$$SS_{Tot} = SS_{Reg} + SS_{Error} \quad (9)$$

$$F_{calc.} = \frac{MSS_{Reg}}{MSS_{Error}} \quad (10)$$

$$F_c = F_{\alpha, df_{Model}, df_{Error}} \quad (11)$$

$$P - value = 2 \times \int_{F_c}^{+\infty} f(F)df \quad (12)$$

$$R^2_{adj} = 1 - \frac{SS_{Error}/_{n-p}}{SS_{Total}/_{n-1}} \quad (13)$$

Where n and p are the numbers of observations and parameters of the model, respectively.

Table (16) - Analysis of variance for a fitted mathematical model to an experimental data using multiple regression [90]

Variation source	Sum of the square	Degree of freedom	Mean sum of the square
Regression	$SS_{Reg} = \sum_j^J \sum_i^{I_j} (\hat{y}_i - \bar{y})^2$ (14)	p-1	$MSS_{Reg} = \frac{SS_{Reg}}{p-1}$ (15)
Error	$SS_{Error} = \sum_j^J \sum_i^{I_j} (y_{ij} - \bar{y}_i)^2$ (16)	n-p	$MSS_{Error} = \frac{SS_{Error}}{n-p}$ (17)
Total	$SS_{Total} = \sum_j^J \sum_i^{I_j} (y_{ij} - \bar{y})^2$ (18)	n-1	-

n: Number of observations, p: Number of the parameters of the model, $\hat{y}_i$: Estimated value for the level i by the model, $\bar{y}$: Mean of overall data, y_{ij}: Replication in each level, $\bar{y}_i$: Mean of replicated data in the same conditions

Biosorption kinetics

Kinetic studies were performed to evaluate the reaction rate, equilibrium time, equilibrium capacity, and biosorption process behavior. For this purpose, the models such as pseudo-second-order and intraparticle diffusion were used according to Equations 19-20, which are shown in Table 17.

Table (17) - Kinetic models using in this study

Model	Equation	Plots	Parameters	Ref.
Pseudo-second-order	$\frac{t}{q_t} = \frac{1}{k_2 q_e^2} + \frac{t}{q_e}$ (19)	$\frac{t}{q_t}$ vs. t	Calculating q_e and k_2 through the slope and intercept	[91]
Intraparticle diffusion	$q_t = k_{id} t^{0.5} + C$ (20)	q_t vs. $t^{0.5}$	Calculating k_{id} and C through the slope and intercept	[92]

Biosorption isotherms

The trend of equilibrium biosorption capacity (q_e) according to the equilibrium concentration of MB (C_e) is investigated using biosorption equilibrium isotherms. The datasets were calculated in different initial concentrations of MB at constant temperatures over time. In each step, q_e was calculated using the biosorption capacity of MDCV/Fe_3O_4. Then C_e was calculated using C_0 and q_e at each run. Langmuir, Freundlich, and Temkin isotherms were examined using Equations 21-24 reported in Table 18 [67, 93, 94].

Table (18) - Isotherm models using in this study

Model	Equation		Plots	Parameters	Ref.
Langmuir	$\frac{C_e}{q_e} = \frac{1}{K_L q_m} + \frac{C_e}{q_m}$	(21)	$\frac{C_e}{q_e}$ vs. C_e	Calculating q_m and K_L through the slope and intercept	[95]
	$R_L = \frac{1}{1+K_L C_0}$	(22)	R_L vs. C_0	R_L	[92]
Freundlich	$\log q_e = \log K_F + \frac{1}{n}\log C_e$	(23)	$\log q_e$ vs. $\log C_e$	Calculating n and K_F through the slope and intercept	[96]
Temkin	$q_e = \frac{RT}{b_T}\ln(K_T) + \frac{RT}{b_T}\ln(C_e)$	(24)	q_e vs. $\ln(C_e)$	Calculating b_T and K_T through the slope and intercept	[97]

Biosorption thermodynamics

The thermodynamics of biosorption of MB on MDCV/Fe_3O_4 were studied at temperatures of 278, 298, and 317 K. Gibbs free energy change (ΔG), enthalpy change (ΔH), and entropy change (ΔS) were calculated according to the following Equations:

$$\Delta G^\circ = \Delta H^\circ - T\Delta S^\circ \quad (25)$$

$$\Delta G^\circ = -RT\ln(K_c) \quad (26)$$

$$\ln(K_c) = \frac{\Delta S^\circ}{R} - \frac{\Delta H^\circ}{RT} \quad (27)$$

$$K_c = \frac{K_F \rho}{1000}\left(\frac{10^6}{\rho}\right)^{(1-\frac{1}{n})} \quad (28)$$

In the above equations, R is the gas constant (J/mol.K), T is the temperature of the process (K), ρ is water density (g/mL), K_F is the Freundlich constant ($(\frac{mg}{g})(\frac{mg}{L})^{1/n}$), n is the Freundlich constant too, and K_c is the equilibrium constant. Equation 27 refers to the Van't Hoff plot of ln K_c versus 1/T [98, 99].

Biosorbent characterization

Several analyses were performed to determine the morphology and specifications of four samples of RCV, DCV, MDCV, and MDCV/Fe_3O_4. The X-ray Diffraction Patterns (XRD) was done by PW1730, PHILIPS, Netherland with Cu-ka radiation and wavelength of 1.54056 A°, at 40 kV in the range of $10 - 80^{\circ}$ with a scanning speed of 0.05°/s. Fourier Transform Infrared Spectroscopy (FTIR) AVATAR, Thermo, USA was used in the range of 400 to 4000 cm^{-1} to identify functional groups. Phase identification, percentage of elements, and morphology of samples were performed using Scanning Electron Microscopy (SEM) and Energy-Dispersive X-ray Spectroscopy (EDS) analyses by MIRA III, TESCAN, Czech Republic. Brunauer-Emmett-Teller (BET) analysis was performed using the liquid nitrogen adsorption-desorption process at 77 K by BELSORP MINI II, BEL, Japan to determine the porosity of the structure. Vibrating Sample Magnetometer (VSM) analysis by Meghnatis Daghigh Kavir Co., Iran at -15000 to 15000 Oe was used to study magnetic properties. The UV-Visible spectrophotometer was also used to determine the MB concentration.

Abbreviations

RCV: Raw *Chlorella vulgaris*, DCV: Defatted *Chlorella vulgaris*, MDCV: Modified defatted *Chlorella vulgaris*, MDCV/Fe_3O_4: Magnetic modified defatted *Chlorella vulgaris*, Fe_3O_4: Iron oxide particles, MB: Methylene blue, CCD: Central composite design, RSM: Response surface methodology, q_{MDCV}: MDCV biosorption capacity, RP_{MDCV}: Residual MDCV, q_{MDCV/Fe_3O_4}: Biosorption capacity of MDCV/Fe_3O_4, q_t: Biosorption capacity, C_0: Initial concentrations of MB, C_t: Final concentrations of MB, ANOVA: Analysis of variance, SS_{Total}: Total sum of the square, SS_{Reg}: Sum of the square of regression, SS_{Error}: Sum of the square of error, $F_{calc.}$: Calculated Fisher distribution, F_c: Critical Fisher distribution, P-value: Probability value, $R^2_{adj.}$: Adjusted determination coefficient, q_e: Equilibrium biosorption capacity, C_e: Equilibrium concentration of MB, ΔG: Gibbs free energy change, ΔH: Enthalpy change, ΔS: Entropy change, XRD: X-ray Diffraction Patterns, FTIR: Fourier Transform Infrared Spectroscopy, SEM: Scanning Electron Microscopy, EDS: Energy-Dispersive X-ray Spectroscopy, BET: Brunauer-Emmett-Teller, VSM: Vibrating Sample Magnetometer, BJH: Barrett-Joyner-Halenda, IUPAC: International Union of Pure and Applied Chemistry.

Acknowledgments

We would like to thank the university of Tehran.

Authors' contributions

Naziri S. wrote the main manuscript text and was involved in all tests directly. Salehi Z. was a chemical engineering supervisor of the research. She also edited the manuscript, sponsored the study, and made all the arrangements.

Funding

It was not a funded project.

Availability of data and materials

All data generated or analyzed during this study are included in the manuscript.

Ethics approval and consent to participate

Not applicable.

Consent for publication

All authors are agree with submission to journal of *Biotechnology for Biofuel*.

Competing interests

There are no competing interests associated with this manuscript.

Author details

[1] Department of Chemical Engineering, School of Chemical Engineering, College of Engineering, University of Tehran, Tehran, Iran.[2] Department of Biotechnology Engineering, School of Chemical Engineering, College of Engineering, University of Tehran, Tehran, Iran

References

[1] M. Goswami and P. Phukan, "Enhanced adsorption of cationic dyes using sulfonic acid modified activated carbon," *Journal of Environmental Chemical Engineering,* vol. 5, no. 4, pp. 3508-3517, 2017.

[2] A. H. Shalla, M. A. Bhat, and Z. Yaseen, "Hydrogels for removal of recalcitrant organic dyes: A conceptual overview," *Journal of environmental chemical engineering,* vol. 6, no. 5, pp. 5938-5949, 2018.

[3] J. Hoslett, H. Ghazal, N. Mohamad, and H. Jouhara, "Removal of methylene blue from aqueous solutions by biochar prepared from the pyrolysis of mixed municipal discarded material," *Science of The Total Environment,* vol. 714, p. 136832, 2020.

[4] G. O. El-Sayed, "Removal of methylene blue and crystal violet from aqueous solutions by palm kernel fiber," *Desalination,* vol. 272, no. 1-3, pp. 225-232, 2011.

[5] M. Rafatullah, O. Sulaiman, R. Hashim, and A. Ahmad, "Adsorption of methylene blue on low-cost adsorbents: a review," *Journal of hazardous materials,* vol. 177, no. 1-3, pp. 70-80, 2010.

[6] J. Ma, X. Tang, Y. He, Y. Fan, and J. Chen, "Robust stable MoS2/GO filtration membrane for effective removal of dyes and salts from water with enhanced permeability," *Desalination,* vol. 480, p. 114328, 2020.

[7] T. A. Aragaw, "Utilizations of electro-coagulated sludge from wastewater treatment plant data as an adsorbent for direct red 28 dye removal," *Data in brief,* vol. 28, p. 104848, 2020.

[8] R. Melo, E. B. Neto, S. Nunes, T. C. Dantas, and A. D. Neto, "Removal of Reactive Blue 14 dye using micellar solubilization followed by ionic flocculation of surfactants," *Separation And Purification Technology,* vol. 191, pp. 161-166, 2018.

[9] V. S. Garcia, J. M. Rosa, and S. I. Borrely, "Toxicity and color reduction of a textile effluent containing reactive red 239 dye by electron beam irradiation," *Radiation Physics and Chemistry,* vol. 172, p. 108765, 2020.

[10] B. O. Unal *et al.*, "Adsorption and Fenton oxidation of azo dyes by magnetite nanoparticles deposited on a glass substrate," *Journal of Water Process Engineering,* vol. 32, p. 100897, 2019.

[11] S. P. Ghuge and A. K. Saroha, "Catalytic ozonation of dye industry effluent using mesoporous bimetallic Ru-Cu/SBA-15 catalyst," *Process Safety and Environmental Protection,* vol. 118, pp. 125-132, 2018.

[12] B. Bharathiraja, I. A. E. Selvakumari, J. Iyyappan, and S. Varjani, "Itaconic acid: an effective sorbent for removal of pollutants from dye industry effluents," *Current Opinion in Environmental Science & Health,* vol. 12, pp. 6-17, 2019.

[13] N. D. Shooto, C. S. Nkutha, N. R. Guilande, and E. B. Naidoo, "Pristine and modified mucuna beans adsorptive studies of toxic lead ions and methylene blue dye from aqueous solution," *South African Journal of Chemical Engineering,* vol. 31, pp. 33-43, 2020.

[14] A. Stavrinou, C. Aggelopoulos, and C. Tsakiroglou, "Exploring the adsorption mechanisms of cationic and anionic dyes onto agricultural waste peels of banana, cucumber and potato: Adsorption kinetics and equilibrium isotherms as a tool," *Journal of environmental chemical engineering,* vol. 6, no. 6, pp. 6958-6970, 2018.

[15] M. Karthika and M. Vasuki, "Adsorption of Alizarine Red-S Dye from Aqueous Solution by Sago Waste: Resolution of Isotherm, Kinetics and Thermodynamics," *Materials Today: Proceedings,* vol. 14, pp. 358-367, 2019.

[16] P. V. Rao, P. Pydiraju, V. Madhuri, S. Vineeth, S. Rahimuddin, and M. Vangalapati, "Removal of indigo carmine dye from aqueous solution by adsorption on biomass of Grevillea Robusta leaves," *Materials Today: Proceedings,* 2020.

[17] Z. Jiang and D. Hu, "Molecular mechanism of anionic dyes adsorption on cationized rice husk cellulose from agricultural wastes," *Journal of Molecular Liquids,* vol. 276, pp. 105-114, 2019.

[18] W. Tsai, J. Yang, C. Lai, Y. Cheng, C. Lin, and C. Yeh, "Characterization and adsorption properties of eggshells and eggshell membrane," *Bioresource technology,* vol. 97, no. 3, pp. 488-493, 2006.

[19] R. M. Moghazy, A. Labena, and S. Husien, "Eco-friendly complementary biosorption process of methylene blue using micro-sized dried biosorbents of two macro-algal species (Ulva fasciata and Sargassum dentifolium): Full factorial design, equilibrium, and kinetic studies," *International journal of biological macromolecules,* vol. 134, pp. 330-343, 2019.

[20] A. L. D. da Rosa, E. Carissimi, G. L. Dotto, H. Sander, and L. A. Feris, "Biosorption of rhodamine B dye from dyeing stones effluents using the green microalgae Chlorella pyrenoidosa," *Journal of Cleaner Production,* vol. 198, pp. 1302-1310, 2018.

[21] F. Afshariani and A. Roosta, "Experimental study and mathematical modeling of biosorption of methylene blue from aqueous solution in a packed bed of microalgae Scenedesmus," *Journal of Cleaner Production,* vol. 225, pp. 133-142, 2019.

[22] D. C. Alves, B. B. Coseglio, L. A. Pinto, and T. R. Cadaval Jr, "Development of Spirulina/chitosan foam adsorbent for phenol adsorption," *Journal of Molecular Liquids,* p. 113256, 2020.

[23] M. A. Maksoud, A. M. Elgarahy, C. Farrell, H. Ala'a, D. W. Rooney, and A. I. Osman, "Insight on water remediation application using magnetic nanomaterials and biosorbents," *Coordination Chemistry Reviews,* vol. 403, p. 213096, 2020.

[24] C. Safi, B. Zebib, O. Merah, P.-Y. Pontalier, and C. Vaca-Garcia, "Morphology, composition, production, processing and applications of Chlorella vulgaris: A review," *Renewable and Sustainable Energy Reviews,* vol. 35, pp. 265-278, 2014.

[25] H. Sati, M. Mitra, S. Mishra, and P. Baredar, "Microalgal lipid extraction strategies for biodiesel production: A review," *Algal Research,* vol. 38, p. 101413, 2019.

[26] J. T. da Fontoura, G. S. Rolim, B. Mella, M. Farenzena, and M. Gutterres, "Defatted microalgal biomass as biosorbent for the removal of Acid Blue 161 dye from tannery effluent," *Journal of environmental chemical engineering,* vol. 5, no. 5, pp. 5076-5084, 2017.

[27] E. Baldikova *et al.*, "Use of waste Japonochytrium sp. biomass after lipid extraction as an efficient adsorbent for triphenylmethane dye applied in aquaculture," *Biomass Conversion and Biorefinery,* vol. 9, no. 3, pp. 479-488, 2019.

[28] H. Shao, Y. Li, L. Zheng, T. Chen, and J. Liu, "Removal of methylene blue by chemically modified defatted brown algae Laminaria japonica," *Journal of the Taiwan Institute of Chemical Engineers,* vol. 80, pp. 525-532, 2017.

[29] E. Daneshvar, A. Vazirzadeh, A. Niazi, M. Sillanpää, and A. Bhatnagar, "A comparative study of methylene blue biosorption using different modified brown, red and green macroalgae–Effect of pretreatment," *Chemical Engineering Journal,* vol. 307, pp. 435-446, 2017.

[30] R. Angelova, E. Baldikova, K. Pospiskova, Z. Maderova, M. Safarikova, and I. Safarik, "Magnetically modified Sargassum horneri biomass as an adsorbent for organic dye removal," *Journal of Cleaner Production,* vol. 137, pp. 189-194, 2016.

[31] S. Mullerova, E. Baldikova, J. Prochazkova, K. Pospiskova, and I. Safarik, "Magnetically modified macroalgae Cymopolia barbata biomass as an adsorbent for safranin O removal," *Materials Chemistry and Physics,* vol. 225, pp. 174-180, 2019.

[32] R. Foroutan, R. Mohammadi, J. Razeghi, and B. Ramavandi, "Performance of algal activated carbon/Fe3O4 magnetic composite for cationic dyes removal from aqueous solutions," *Algal Research,* vol. 40, p. 101509, 2019.

[33] M. T. Bai and P. Venkateswarlu, "Optimization studies for lead biosorption on Sargassum tenerrimum (Brown Algae) using experimental design: Response Surface Methodology," *Materials Today: Proceedings,* vol. 18, pp. 4290-4298, 2019.

[34] G. Falini, S. Fermani, M. Gazzano, and A. Ripamonti, "Structure and morphology of synthetic magnesium calcite," *Journal of Materials Chemistry,* vol. 8, no. 4, pp. 1061-1065, 1998.

[35] P. Althoff, "Structural refinements of dolomite and a magnesian calcite and implications for dolomite formation in the marine environment," *American Mineralogist,* vol. 62, no. 7-8, pp. 772-783, 1977.

[36] S. Sasaki, "Radial distribution of electron density in magnetite, Fe3O4," *Acta Crystallographica Section B: Structural Science,* vol. 53, no. 5, pp. 762-766, 1997.

[37] A. C. Khorasani and S. A. Shojaosadati, "Magnetic pectin-Chlorella vulgaris biosorbent for the adsorption of dyes," *Journal of Environmental Chemical Engineering,* vol. 7, no. 3, p. 103062, 2019.

[38] T. Driver, A. K. Bajhaiya, J. W. Allwood, R. Goodacre, J. K. Pittman, and A. P. Dean, "Metabolic responses of eukaryotic microalgae to environmental stress limit the ability of FT-IR spectroscopy for species identification," *Algal research,* vol. 11, pp. 148-155, 2015.

[39] K. Maliutina, A. Tahmasebi, and J. Yu, "The transformation of nitrogen during pressurized entrained-flow pyrolysis of Chlorella vulgaris," *Bioresource technology,* vol. 262, pp. 90-97, 2018.

[40] Y. Wang, Y. Zhang, S. Li, W. Zhong, and W. Wei, "Enhanced methylene blue adsorption onto activated reed-derived biochar by tannic acid," *Journal of Molecular Liquids,* vol. 268, pp. 658-666, 2018.

[41] Y. Peng *et al.*, "Enhanced Hg (II) adsorption by monocarboxylic-acid-modified microalgae residuals in simulated and practical industrial wastewater," *Energy & Fuels,* vol. 32, no. 4, pp. 4461-4468, 2018.

[42] Y. Lebron, V. Moreira, and L. Santos, "Studies on dye biosorption enhancement by chemically modified Fucus vesiculosus, Spirulina maxima and Chlorella pyrenoidosa algae," *Journal of Cleaner Production,* vol. 240, p. 118197, 2019.

[43] P. L. Gupta, H. Jung, D. Tiwari, S.-H. Kong, and S.-M. Lee, "Insight into the mechanism of Cd (II) and Pb (II) removal by sustainable magnetic biosorbent precursor to Chlorella vulgaris," *Journal of the Taiwan Institute of Chemical Engineers,* vol. 71, pp. 206-213, 2017.

[44] A. Asiedu, R. Davis, and S. Kumar, "Catalytic transfer hydrogenation and characterization of flash hydrolyzed microalgae into hydrocarbon fuels production (jet fuel)," *Fuel,* vol. 261, p. 116440, 2020.

[45] S. Lowell, J. E. Shields, M. A. Thomas, and M. Thommes, *Characterization of porous solids and powders: surface area, pore size and density*. Springer Science & Business Media, 2012.

[46] K. Hwang *et al.*, "Chlamydomonas angulosa (Green Alga) and Nostoc commune (Blue-Green Alga) microalgae-cellulose composite aerogel beads: manufacture, physicochemical characterization, and Cd (II) adsorption," *Materials,* vol. 11, no. 4, p. 562, 2018.

[47] H. Qiu, C. Luo, M. Sun, F. Lu, L. Fan, and X. Li, "A chemiluminescence sensor for determination of epinephrine using graphene oxide–magnetite-molecularly imprinted polymers," *Carbon,* vol. 50, no. 11, pp. 4052-4060, 2012.

[48] M. Govarthanan, C.-H. Jeon, Y.-H. Jeon, J.-H. Kwon, H. Bae, and W. Kim, "Non-toxic nano approach for wastewater treatment using Chlorella vulgaris exopolysaccharides immobilized in iron-magnetic nanoparticles," *International Journal of Biological Macromolecules,* vol. 162, pp. 1241-1249, 2020.

[49] S. Ghosh, A. Badruddoza, M. Uddin, and K. Hidajat, "Adsorption of chiral aromatic amino acids onto carboxymethyl-β-cyclodextrin bonded Fe3O4/SiO2 core–shell nanoparticles," *Journal of colloid and interface science,* vol. 354, no. 2, pp. 483-492, 2011.

[50] S. Khammar, N. Bahramifar, and H. Younesi, "Optimization using the response surface methodology for adsorption of polychlorinated biphenyls (PCBs) from transformer oil by magnetic CMCD-Fe3O4@ SiO2 nanoparticles," *Materials Chemistry and Physics,* p. 123195, 2020.

[51] N. E.-A. El-Naggar and N. H. Rabei, "Bioprocessing optimization for efficient simultaneous removal of methylene blue and nickel by Gracilaria seaweed biomass," *Scientific Reports,* vol. 10, no. 1, pp. 1-21, 2020.

[52] N. Kumari and R. K. Singh, "Biofuel and co-products from algae solvent extraction," *Journal of environmental management,* vol. 247, pp. 196-204, 2019.

[53] P. Sharma, N. Hussain, D. J. Borah, and M. R. Das, "Kinetics and adsorption behavior of the methyl blue at the graphene oxide/reduced graphene oxide nanosheet–water interface: a comparative study," *Journal of Chemical & Engineering Data,* vol. 58, no. 12, pp. 3477-3488, 2013.

[54] P. Nautiyal, K. Subramanian, and M. Dastidar, "Adsorptive removal of dye using biochar derived from residual algae after in-situ transesterification: alternate use of waste of biodiesel industry," *Journal of Environmental Management,* vol. 182, pp. 187-197, 2016.

[55] F. Luo, Y. Liu, X. Li, Z. Xuan, and J. Ma, "Biosorption of lead ion by chemically-modified biomass of marine brown algae Laminaria japonica," *Chemosphere,* vol. 64, no. 7, pp. 1122-1127, 2006.

[56] S. Hadjoudja, V. Deluchat, and M. Baudu, "Cell surface characterisation of Microcystis aeruginosa and Chlorella vulgaris," *Journal of colloid and interface science,* vol. 342, no. 2, pp. 293-299, 2010.

[57] M. Ahmed, P. Okoye, E. Hummadi, and B. Hameed, "High-performance porous biochar from the pyrolysis of natural and renewable seaweed (Gelidiella acerosa) and its application for the adsorption of methylene blue," *Bioresource technology,* vol. 278, pp. 159-164, 2019.

[58] S. Rangabhashiyam and P. Balasubramanian, "Characteristics, performances, equilibrium and kinetic modeling aspects of heavy metal removal using algae," *Bioresource Technology Reports,* vol. 5, pp. 261-279, 2019.

[59] F. Mashkoor and A. Nasar, "Magsorbents: Potential candidates in wastewater treatment technology–A review on the removal of methylene blue dye," *Journal of Magnetism and Magnetic Materials,* vol. 500, p. 166408, 2020.

[60] A. Selvakumar and S. Rangabhashiyam, "Biosorption of Rhodamine B onto novel biosorbents from Kappaphycus alvarezii, Gracilaria salicornia and Gracilaria edulis," *Environmental Pollution,* vol. 255, p. 113291, 2019.

[61] A. Kőnig-Péter, F. Kilár, A. Felinger, and T. Pernyeszi, "Biosorption characteristics of Spirulina and Chlorella cells to accumulate heavy metals," *Journal of the Serbian Chemical Society,* vol. 80, no. 3, pp. 407-419, 2015.

[62] T. A. Khan and E. A. Khan, "Removal of basic dyes from aqueous solution by adsorption onto binary iron-manganese oxide coated kaolinite: non-linear isotherm and kinetics modeling," *Applied Clay Science,* vol. 107, pp. 70-77, 2015.

[63] F.-M. Pellera *et al.*, "Adsorption of Cu (II) ions from aqueous solutions on biochars prepared from agricultural by-products," *Journal of Environmental Management,* vol. 96, no. 1, pp. 35-42, 2012.

[64] A. Pholosi, E. B. Naidoo, and A. E. Ofomaja, "Intraparticle diffusion of Cr (VI) through biomass and magnetite coated biomass: A comparative kinetic and diffusion study," *South African Journal of Chemical Engineering,* vol. 32, pp. 39-55, 2020.

[65] M. Arami, N. Y. Limaee, N. M. Mahmoodi, and N. S. Tabrizi, "Removal of dyes from colored textile wastewater by orange peel adsorbent: equilibrium and kinetic studies," *Journal of Colloid and interface Science,* vol. 288, no. 2, pp. 371-376, 2005.

[66] U. Kumar and M. Bandyopadhyay, "Sorption of cadmium from aqueous solution using pretreated rice husk," *Bioresource technology,* vol. 97, no. 1, pp. 104-109, 2006.

[67] K. Y. Foo and B. H. Hameed, "Insights into the modeling of adsorption isotherm systems," *Chemical engineering journal,* vol. 156, no. 1, pp. 2-10, 2010.

[68] L. A. Rodrigues, M. L. C. P. da Silva, M. O. Alvarez-Mendes, A. dos Reis Coutinho, and G. P. Thim, "Phenol removal from aqueous solution by activated carbon produced from avocado kernel seeds," *Chemical Engineering Journal,* vol. 174, no. 1, pp. 49-57, 2011.

[69] Z. Bekçi, Y. Seki, and M. K. Yurdakoç, "Equilibrium studies for trimethoprim adsorption on montmorillonite KSF," *Journal of Hazardous Materials,* vol. 133, no. 1-3, pp. 233-242, 2006.

[70] S. Cheng *et al.*, "Adsorption behavior of methylene blue onto waste-derived adsorbent and exhaust gases recycling," *RSC advances,* vol. 7, no. 44, pp. 27331-27341, 2017.

[71] T. Egbosiuba *et al.*, "Ultrasonic enhanced adsorption of methylene blue onto the optimized surface area of activated carbon: Adsorption isotherm, kinetics and thermodynamics," *Chemical Engineering Research and Design,* vol. 153, pp. 315-336, 2020.

[72] M. Ncibi *et al.*, "Biosorptive uptake of methylene blue using Mediterranean green alga Enteromorpha spp," *Journal of Hazardous Materials,* vol. 170, no. 2-3, pp. 1050-1055, 2009.

[73] E. Daneshvar, A. Vazirzadeh, and A. Bhatnagar, "Biosorption of methylene blue dye onto three different marine macroalgae: Effects of different parameters on isotherm, kinetic and thermodynamic," *Iranian Journal of Science and Technology, Transactions A: Science,* vol. 43, no. 6, pp. 2743-2754, 2019.

[74] X. Yao *et al.*, "Magnetic activated biochar nanocomposites derived from wakame and its application in methylene blue adsorption," *Bioresource Technology,* vol. 302, p. 122842, 2020.

[75] N. Sebeia, M. Jabli, A. Ghith, Y. Elghoul, and F. M. Alminderej, "Production of cellulose from Aegagropila Linnaei macro-algae: Chemical modification, characterization and application for the bio-sorptionof cationic and anionic dyes from water," *International journal of biological macromolecules,* vol. 135, pp. 152-162, 2019.

[76] M. L. F. A. De Castro, M. L. B. Abad, D. A. G. Sumalinog, R. R. M. Abarca, P. Paoprasert, and M. D. G. de Luna, "Adsorption of methylene blue dye and Cu (II) ions on EDTA-modified bentonite: isotherm, kinetic and thermodynamic studies," *Sustainable Environment Research,* vol. 28, no. 5, pp. 197-205, 2018.

[77] L. Zeghoud, M. Gouamid, O. B. Mya, A. Rebiai, and M. Saidi, "Adsorption of methylene blue dye from aqueous solutions using two different parts of palm tree: palm frond base and palm leaflets," *Water, Air, & Soil Pollution,* vol. 230, no. 8, p. 195, 2019.

[78] D. Caparkaya and L. Cavas, "Biosorption of Methylene Blue by a Brown Alga Cystoseira barbatula Kützing," *Acta Chimica Slovenica,* vol. 55, no. 3, 2008.

[79] J. Y. Chin, L. M. Chng, S. S. Leong, S. P. Yeap, N. H. M. Yasin, and P. Y. Toh, "Removal of Synthetic Dye by Chlorella vulgaris Microalgae as Natural Adsorbent," *ARABIAN JOURNAL FOR SCIENCE AND ENGINEERING,* 2020.

[80] T. Santhi, S. Manonmani, V. Vasantha, and Y. Chang, "A new alternative adsorbent for the removal of cationic dyes from aqueous solution," *Arabian journal of chemistry,* vol. 9, pp. S466-S474, 2016.

[81] T. S. Chandra *et al.*, "Defatted algal biomass as a non-conventional low-cost adsorbent: surface characterization and methylene blue adsorption characteristics," *Bioresource technology,* vol. 184, pp. 395-404, 2015.

[82] M. C. Ncibi, B. Mahjoub, and M. Seffen, "Kinetic and equilibrium studies of methylene blue biosorption by Posidonia oceanica (L.) fibres," *Journal of hazardous materials,* vol. 139, no. 2, pp. 280-285, 2007.

[83] S. Cengiz and L. Cavas, "Removal of methylene blue by invasive marine seaweed: Caulerpa racemosa var. cylindracea," *Bioresource Technology,* vol. 99, no. 7, pp. 2357-2363, 2008.

[84] D. Sallet *et al.*, "Ultrasound-assisted extraction of lipids from Mortierella isabellina," *Journal of Food Engineering,* vol. 242, pp. 1-7, 2019.

[85] E. G. Bligh and W. J. Dyer, "A rapid method of total lipid extraction and purification," *Canadian journal of biochemistry and physiology,* vol. 37, no. 8, pp. 911-917, 1959.

[86] A. V. Rane, K. Kanny, V. Abitha, and S. Thomas, "Methods for synthesis of nanoparticles and fabrication of nanocomposites," in *Synthesis of inorganic nanomaterials*: Elsevier, 2018, pp. 121-139.

[87] D. Ramimoghadam, S. Bagheri, and S. B. Abd Hamid, "Progress in electrochemical synthesis of magnetic iron oxide nanoparticles," *Journal of Magnetism and Magnetic Materials,* vol. 368, pp. 207-229, 2014.

[88] T. Nematian, Z. Salehi, and A. Shakeri, "Conversion of bio-oil extracted from Chlorella vulgaris micro algae to biodiesel via modified superparamagnetic nano-biocatalyst," *Renewable Energy,* vol. 146, pp. 1796-1804, 2020.

[89] L. D. Youcef, L. S. Belaroui, and A. López-Galindo, "Adsorption of a cationic methylene blue dye on an Algerian palygorskite," *Applied Clay Science,* vol. 179, p. 105145, 2019.

[90] M. A. Bezerra, R. E. Santelli, E. P. Oliveira, L. S. Villar, and L. A. Escaleira, "Response surface methodology (RSM) as a tool for optimization in analytical chemistry," *Talanta,* vol. 76, no. 5, pp. 965-977, 2008.

[91] Y.-S. Ho and G. McKay, "Pseudo-second order model for sorption processes," *Process biochemistry,* vol. 34, no. 5, pp. 451-465, 1999.

[92] F.-C. Wu, R.-L. Tseng, and R.-S. Juang, "Initial behavior of intraparticle diffusion model used in the description of adsorption kinetics," *Chemical engineering journal,* vol. 153, no. 1-3, pp. 1-8, 2009.

[93] G. Roberts, *Langmuir-blodgett films*. Springer Science & Business Media, 2013.

[94] Y. Cui, A. Masud, N. Aich, and J. D. Atkinson, "Phenol and Cr (VI) removal using materials derived from harmful algal bloom biomass: Characterization and performance assessment for a biosorbent, a porous carbon, and Fe/C composites," *Journal of hazardous materials,* vol. 368, pp. 477-486, 2019.

[95] I. Langmuir, "The constitution and fundamental properties of solids and liquids. Part I. Solids," *Journal of the American chemical society,* vol. 38, no. 11, pp. 2221-2295, 1916.

[96] H. Freundlich, "Over the adsorption in solution," *J. Phys. Chem,* vol. 57, no. 385471, pp. 1100-1107, 1906.

[97] M. Tempkin and V. Pyzhev, "Kinetics of ammonia synthesis on promoted iron catalyst," *Acta Phys. Chim. USSR,* vol. 12, no. 1, p. 327, 1940.

[98] R. Aravindhan, J. R. Rao, and B. U. Nair, "Removal of basic yellow dye from aqueous solution by sorption on green alga Caulerpa scalpelliformis," *Journal of Hazardous Materials,* vol. 142, no. 1-2, pp. 68-76, 2007.

[99] H. N. Tran, S.-J. You, A. Hosseini-Bandegharaei, and H.-P. Chao, "Mistakes and inconsistencies regarding adsorption of contaminants from aqueous solutions: a critical review," *Water research,* vol. 120, pp. 88-116, 2017.

Figures

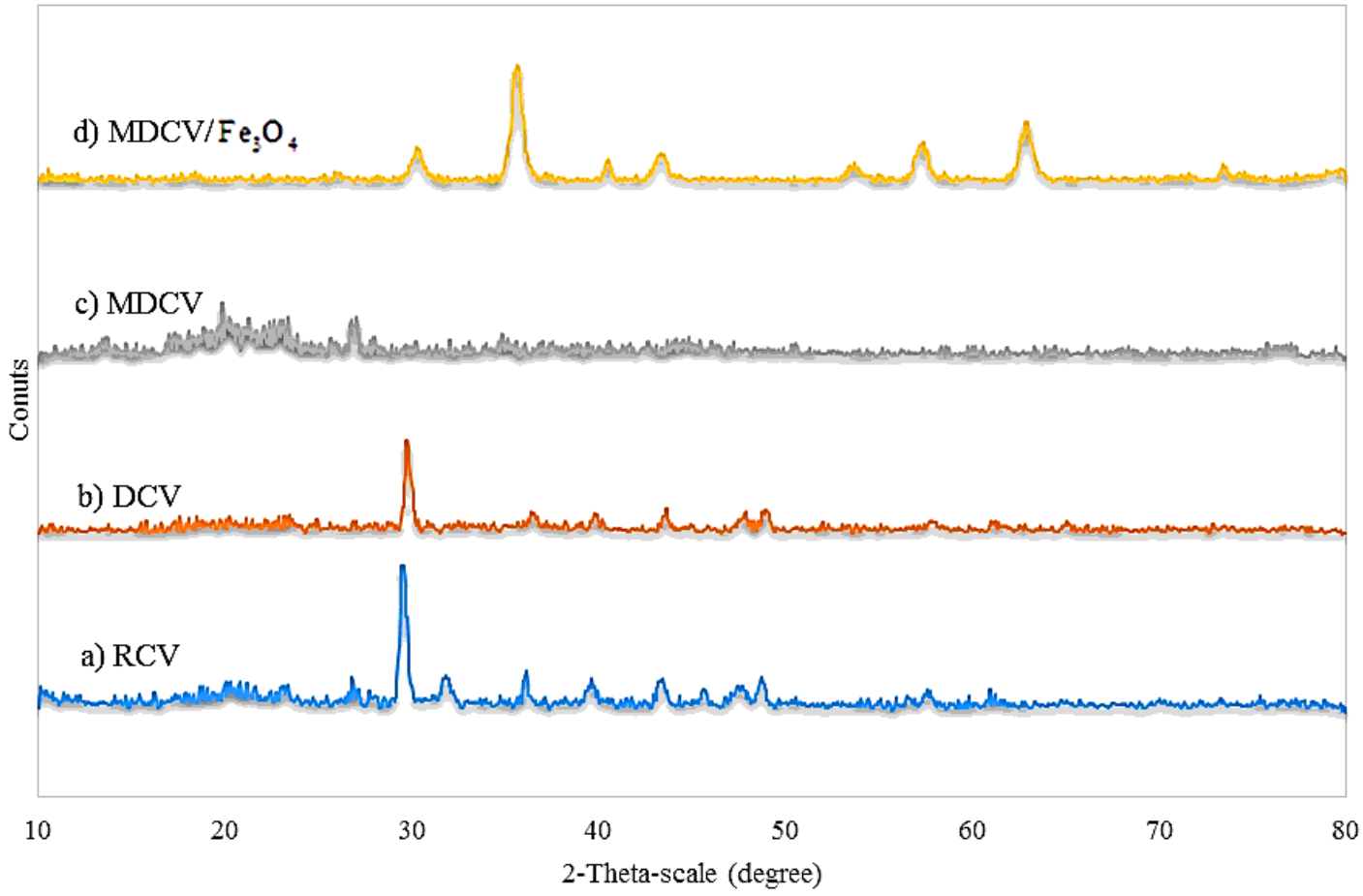

Figure 1

XRD analysis for a) RCV, b) DCV, c) MDCV and d) MDCV/Fe3O4

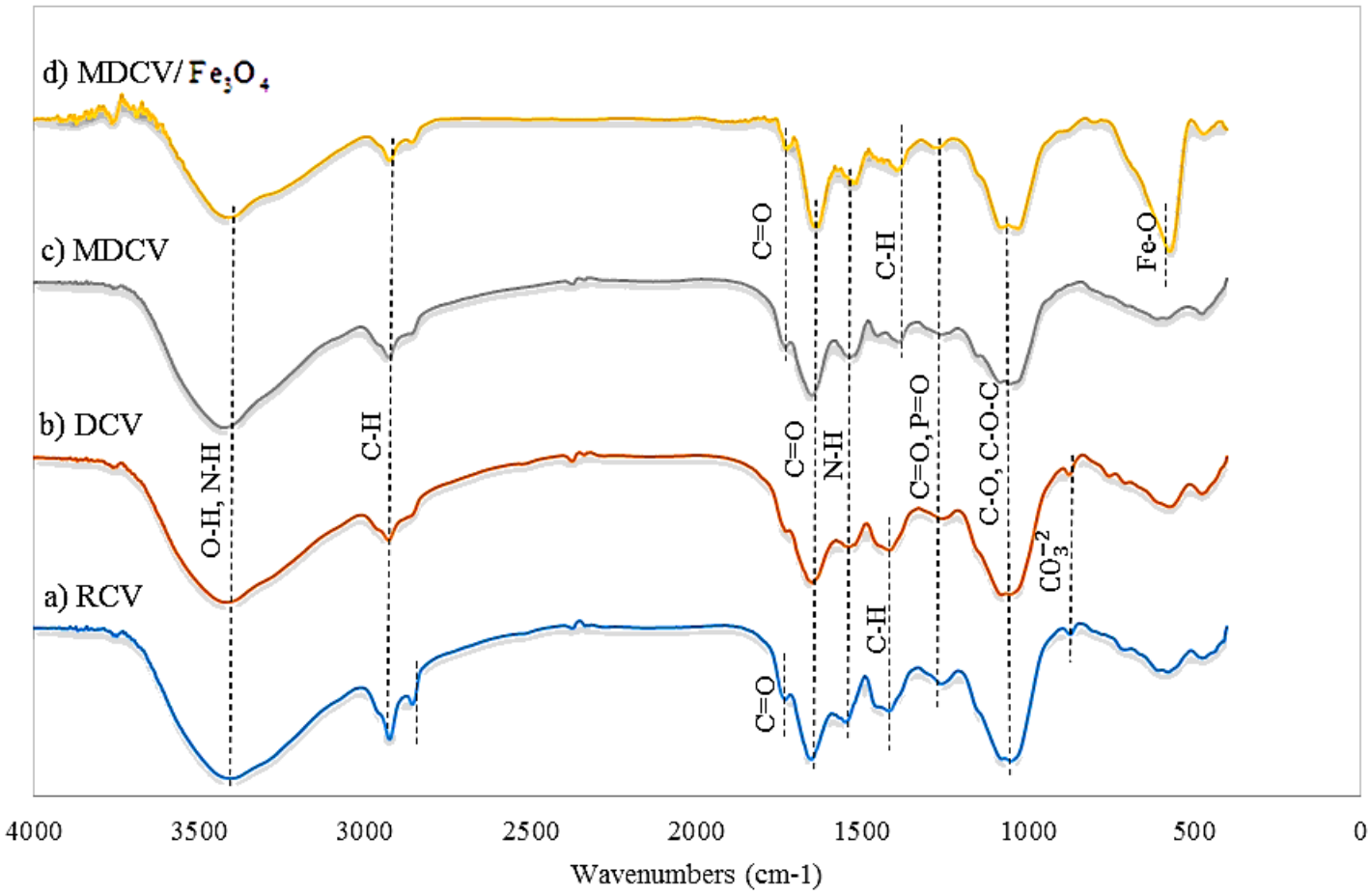

Figure 2

FT-IR analysis for a) RCV, b) DCV, c) MDCV, and d) MDCV/Fe3O4

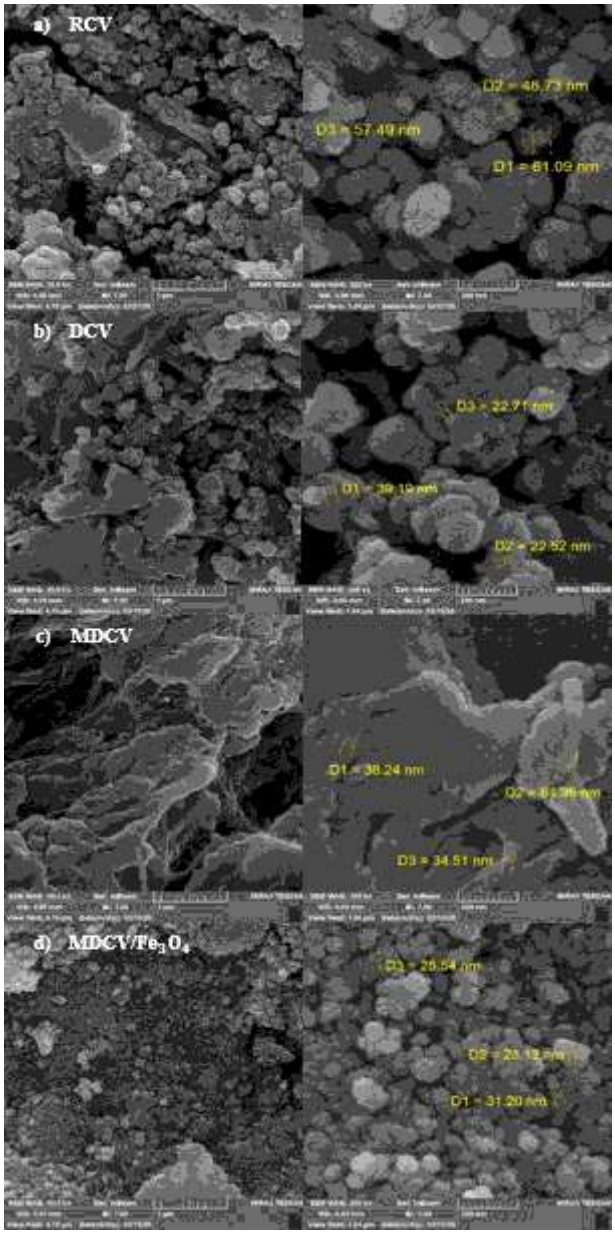

Figure 3

SEM analysis for a) RCV, b) DCV, c) MDCV, and d) MDCV/Fe3O4

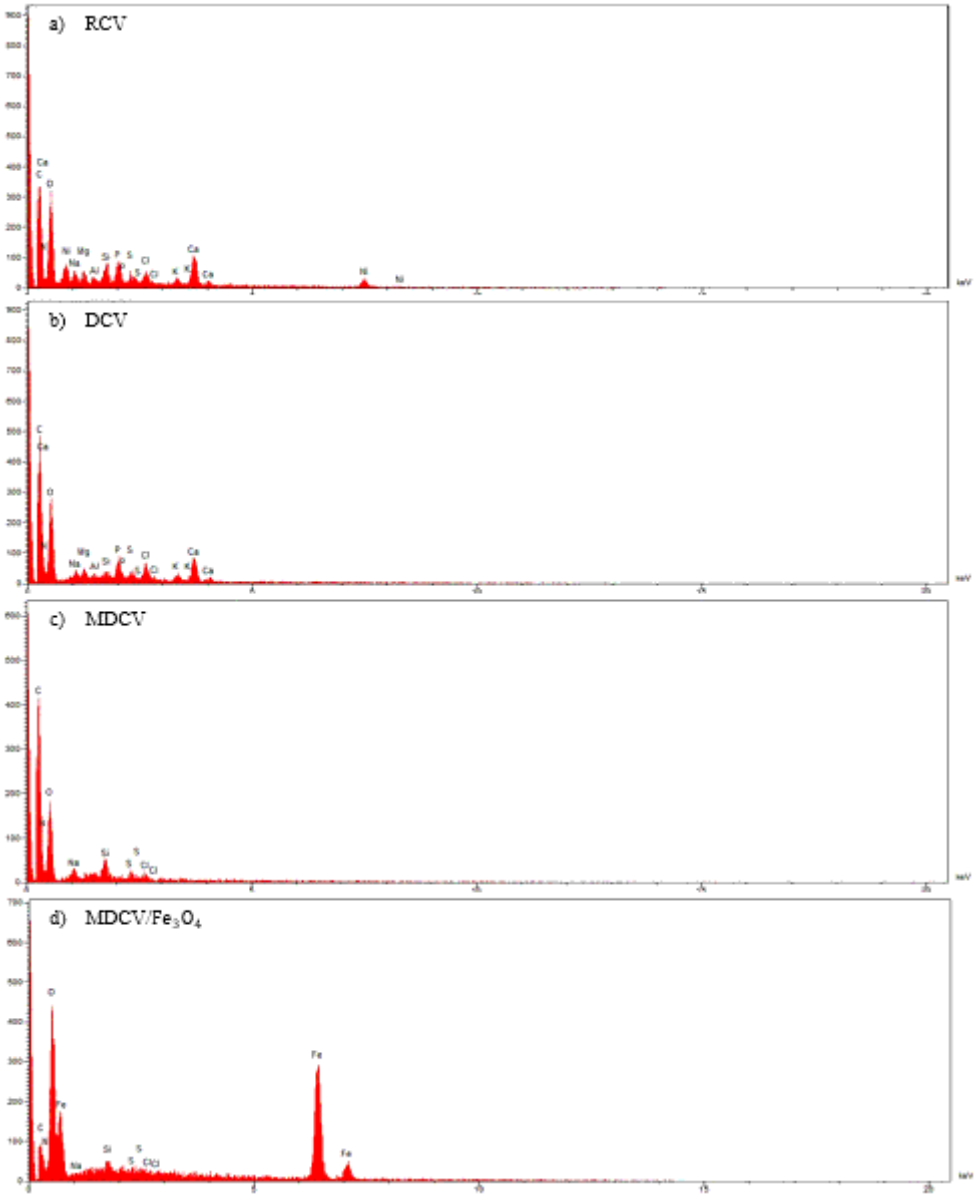

Figure 4

EDS analysis for a) RCV, b) DCV, c) MDCV, and d) MDCV/Fe3O4

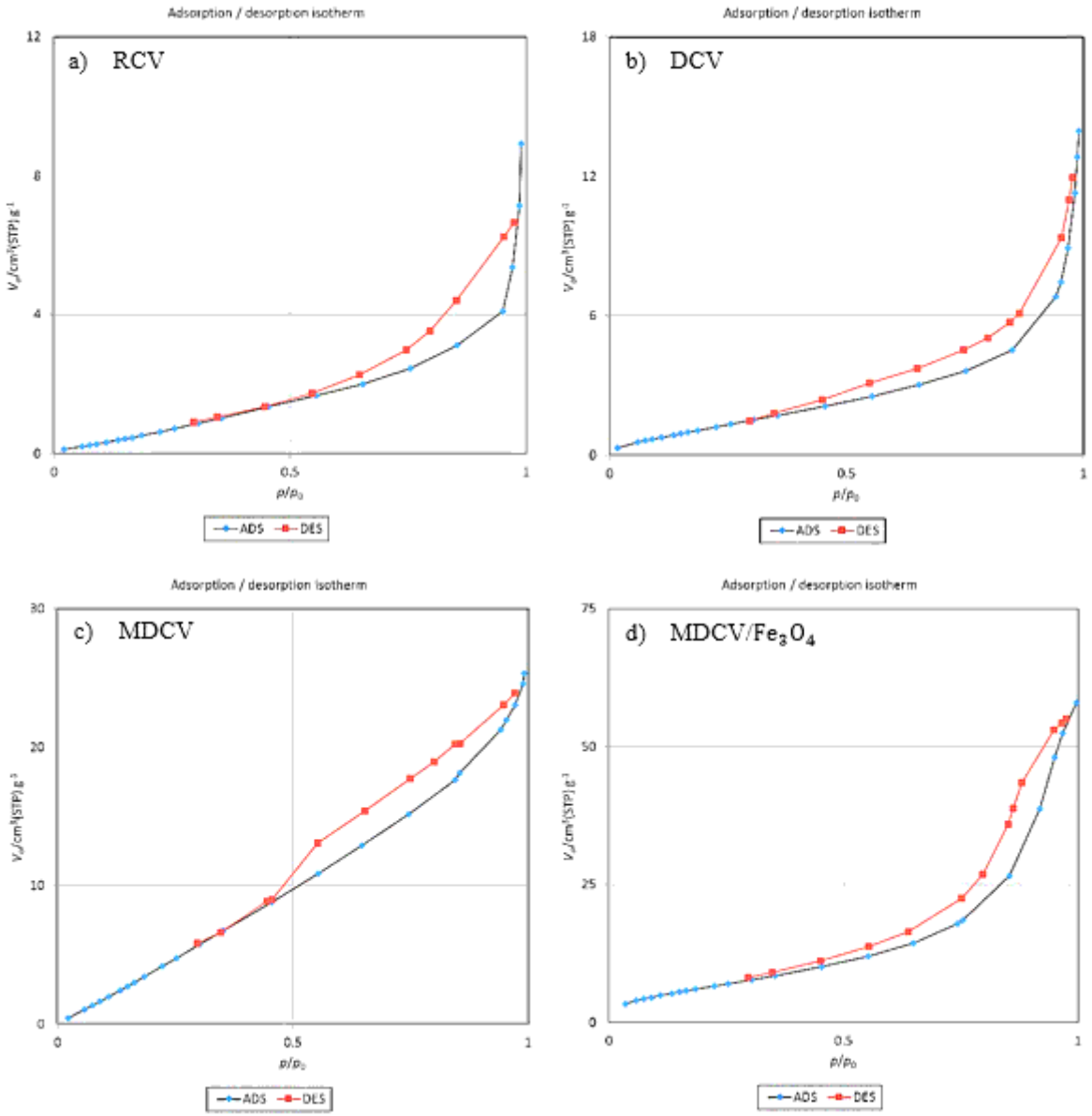

Figure 5

Nitrogen adsorption-desorption isotherm for a) RCV, b) DCV, c) MDCV, and d) MDCV/Fe3O4

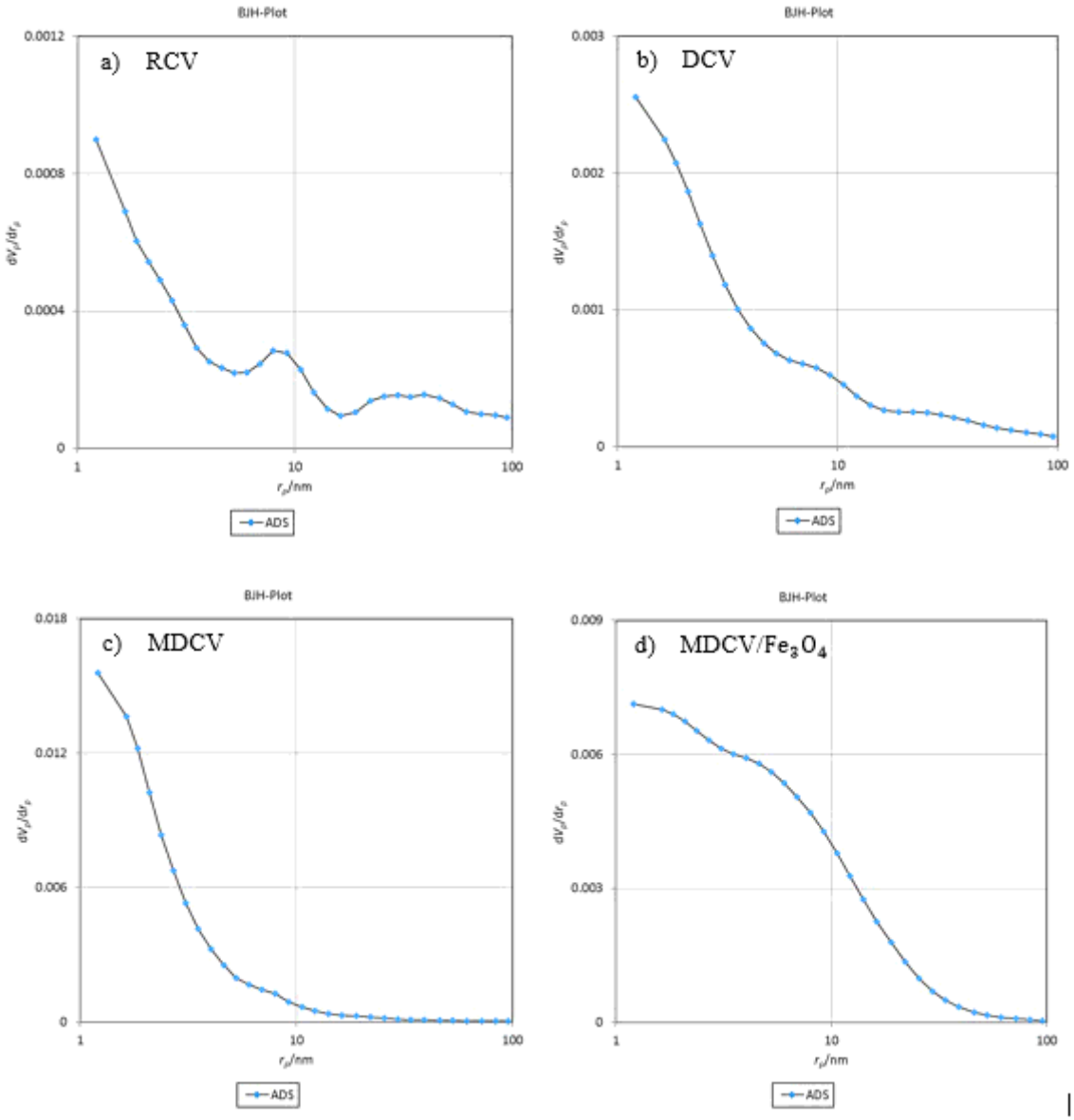

Figure 6

BJH pore size distribution for a) RCV, b) DCV, c) MDCV, and d) MDCV/Fe3O4

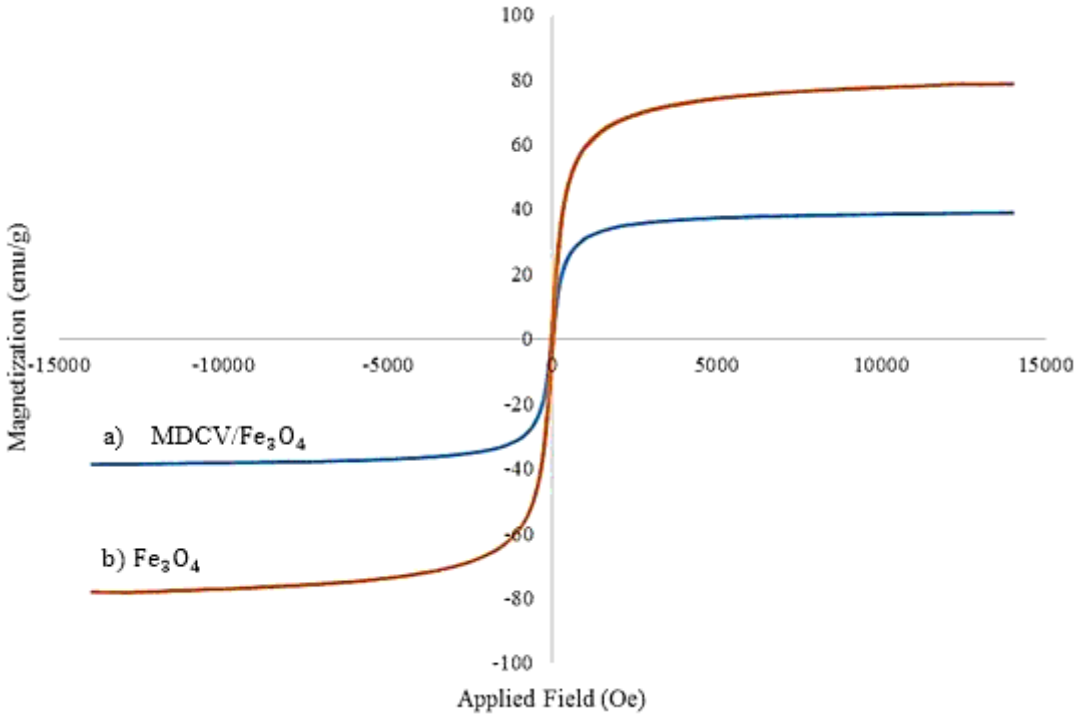

Figure 7

VSM analysis for a) MDCV/Fe_3 O_4, b) Fe3O4

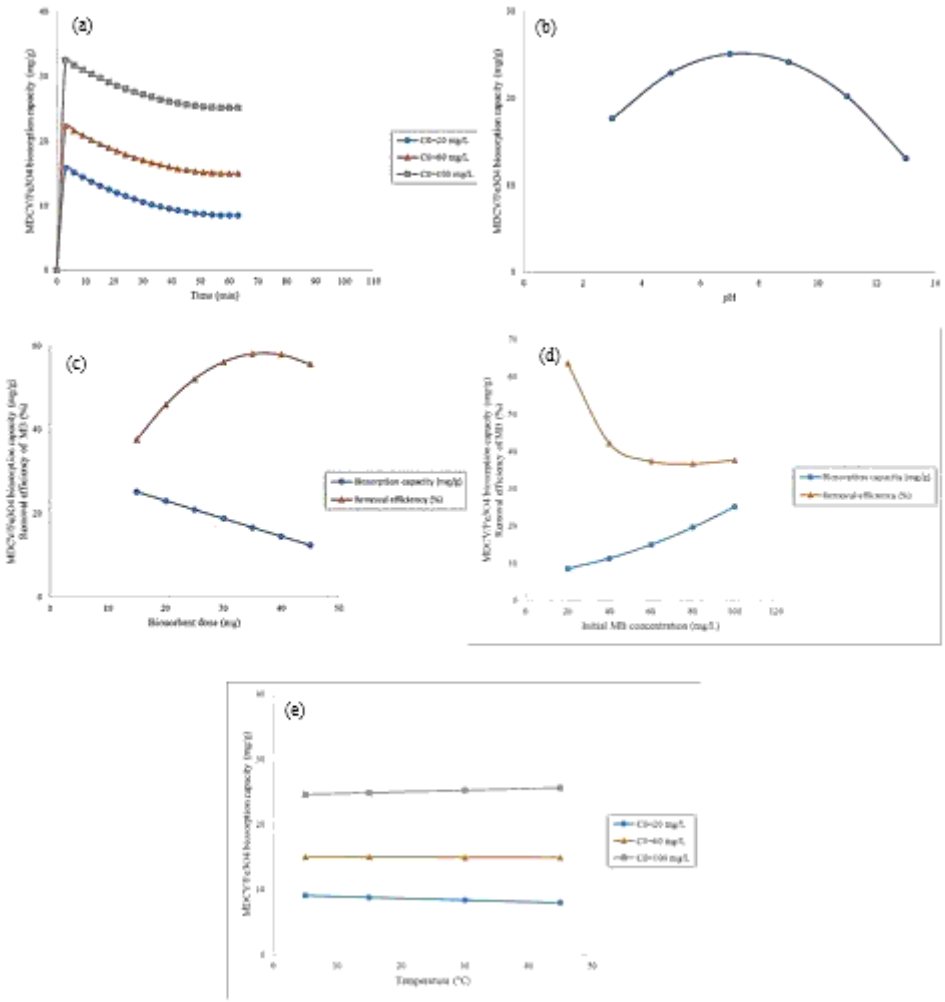

Figure 8

Effect of a) contact time (T=25℃, m=15 mg, pH=7), b) pH (T=25℃, t=60 min, m=15 mg, C0=100 mg/L), c) biosorbent dosage (T=25℃, t= 60 min, C0=100 mg/L, pH=7), d) initial concentration of MB (T=25℃, t=60 min, m=15 mg, pH=7), and e) temperature (t= 60 min, m=15 mg, pH=7) on biosorption of MB by MDCV/Fe3O4

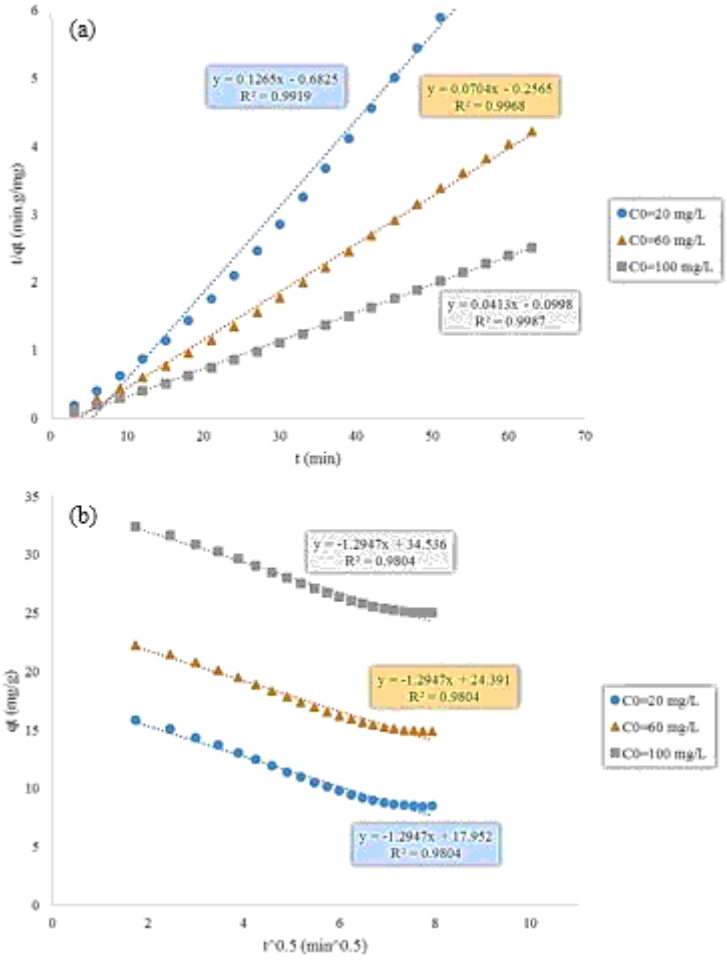

Figure 9

Plots of a) pseudo-second-order, b) intraparticle diffusion kinetic models for MB biosorption onto MDCV/Fe3O4(T=25℃, m=15mg, pH=7)

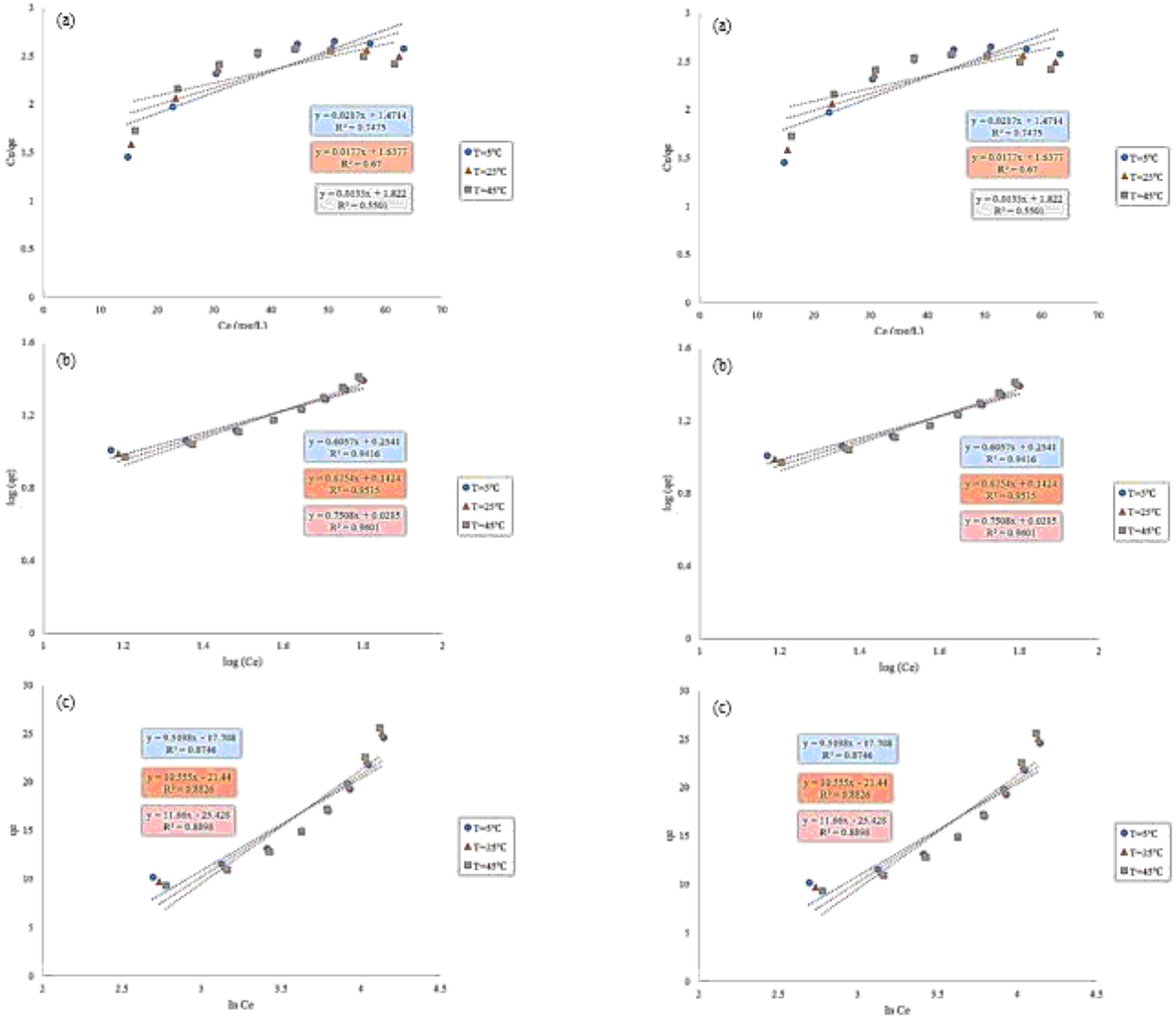

Figure 10

Plots of a) Langmuir, b) Freundlich, c) Temkin isotherm models for MB biosorption onto MDCV/Fe3O4

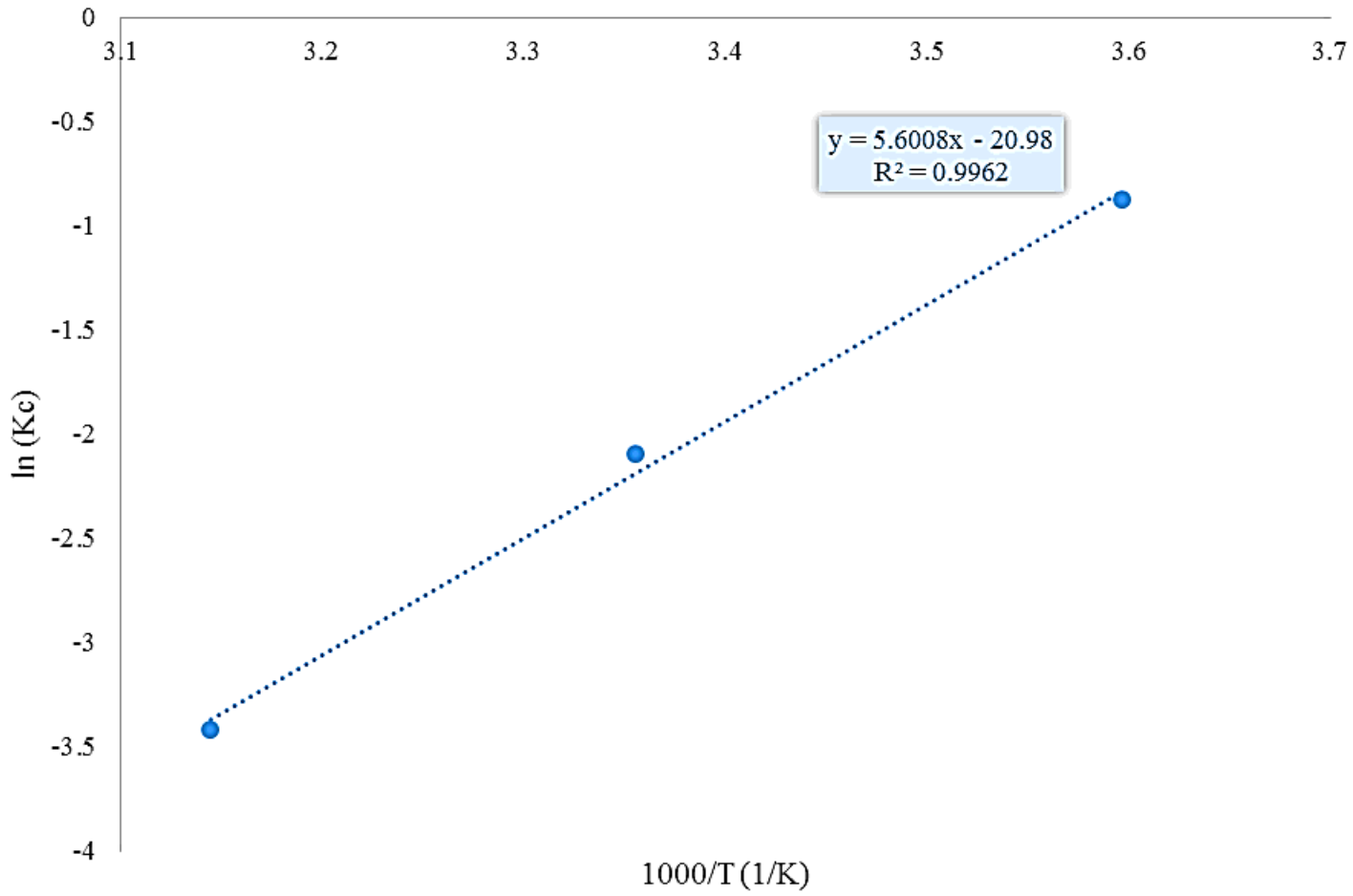

Figure 11

Van't Hoff diagram for the estimation of thermodynamic parameters